P 2mi4

NASA CR-134531

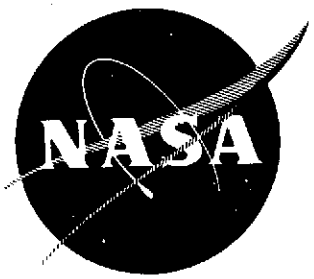

HIGH TEMPERATURE COMPOUNDS FOR TURBINE VANES

by W.H. Rhodes and R.M. Cannon, Jr.

AVCO SYSTEMS DIVISION
Lowell, Massachusetts

AVSD-0006-74-CR

Prepared for

NATIONAL AERONAUTICS AND SPACE ADMINISTRATION

NASA Lewis Research Center
Contract NAS3-16757
William A. Sanders, Project Manager

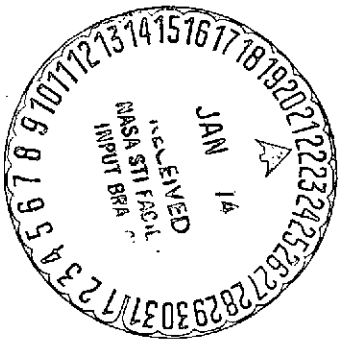

(NASA-CR-134531) HIGH TEMPERATURE COMPOUNDS FOR TURBINE VANES (Avco Corp., Lowell, Mass.) ~~74~~ 67 p HC $5.75 CSCL 11D

N74-15233

Unclas
G3/18 25700

NASA CR-134531

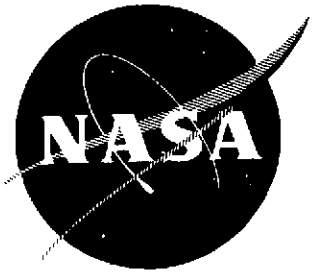

HIGH TEMPERATURE COMPOUNDS FOR TURBINE VANES

by W.H. Rhodes and R.M. Cannon, Jr.

AVCO SYSTEMS DIVISION
Lowell, Massachusetts

AVSD-0006-74-CR

Prepared for

NATIONAL AERONAUTICS AND SPACE ADMINISTRATION

NASA Lewis Research Center
Contract NAS3-16757
William A. Sanders, Project Manager

1. Report No.	2. Government Accession No.	3. Recipient's Catalog No.
NASA CR-134531		

4. Title and Subtitle	5. Report Date
High Temperature Compounds for Turbine Vanes (U)	January 1974
	6. Performing Organization Code

7. Author(s)	8. Performing Organization Report No.
W.H. Rhodes R.M. Cannon, Jr.	AVSD-0006-74-CR
	10. Work Unit No.

9. Performing Organization Name and Address	11. Contract or Grant No.
AVCO Corporation Systems Division Lowell, Mass. 01851	NAS 3-16757
	13. Type of Report and Period Covered
12. Sponsoring Agency Name and Address	Contractor Report
National Aeronautics & Space Administration Washington, D.C. 20546	14. Sponsoring Agency Code

15. Supplementary Notes

Project Manager - William A. Sanders
NASA/Lewis Research Center, Cleveland, Ohio

16. Abstract

Fabrication and microstructure control studies were conducted on SiC, Si_3N_4 and composites based on Si_3N_4. Charpy mode impact testing to 2400°F established that Si_3N_4/Mo composites have excellent potential. Attempts to fabricate composites of Si_3N_4 with superalloys, both by hot pressing and infiltration were largely unsuccessful in comparison to using Mo, Re, and Ta which are less reactive. Modest further improvements in impact strength were realized for monolithic Si_3N_4; however, SiC strengths increased by a factor of six and now equal values achieved for Si_3N_4. Correlations of impact strength with material properties are discussed. Reduced MgO densification aid additions to Si_3N_4 were found to decrease densification kinetics, increase final porosity, decrease room temperature bend strength, increase high temperature bend strength and decrease bend stress rupture properties. The decrease in bend strength at high temperature for fine grain size SiC suggested that a slightly larger grain size material with a nearly constant strength-temperature relation may prove desirable in the creep and stress rupture mode.

17. Key Words (Suggested by Author(s))	18. Distribution Statement
Composites Turbine Materials Ceramics Mechanical Properties of Ceramics Silicon Nitride Silicon Carbide	Unclassified - Unlimited

19. Security Classif. (of this report)	20. Security Classif. (of this page)	21. No. of Pages	22. Price*
Unclassified	Unclassified	66	

* For sale by the National Technical Information Service, Springfield, Virginia 22151

NASA-C-168 (Rev. 6-71)

FOREWORD

The research described herein was conducted by the Avco Corporation, Systems Division, under NASA Contract NAS3-16757. The work was done under the management of the NASA Project Manager, Mr. William A. Sanders, Materials and Structures Division, NASA/Lewis Research Center. Dr. William H. Rhodes was the Principal Investigator with Mr. Rowland M. Cannon, Jr., assisting in materials evaluation. Other Avco personnel who contributed significantly to this project were Philip Foley, Ernest Vallante, John Centorino, Burton MacAllister, Charles Houck, Philip Berneburg, and Donald Sedota.

TABLE OF CONTENTS

LIST OF FIGURES

LIST OF FIGURES cont.

LIST OF TABLES

I. SUMMARY

The objective of this program was to determine the feasibility of improving the mechanical behavior of high temperature composites to such a degree that they may become candidate materials for use as turbine stator vanes and blades in advanced turbine engines. The compounds studied were monolithic SiC and Si_3N_4 and composites based on the Si_3N_4 matrix with metal phases introduced in the form of wires and metallic infiltrations. Areas receiving minor attention were the application of surface coatings and the consolidation of Si_2ON_2. Primary emphasis was given toward improving the mechanical impact resistance at temperatures between 2000°F - 2400°F. The influence of Si_3N_4 microstructures and process variables on bend strength and stress rupture life were also studied. Material development was conducted with a goal of retaining the demonstrated oxidation resistance and thermal shock stability of the matrix.

Si_3N_4/Mo and Si_3N_4/Re with up to 19 v/o of oriented 0.010 inch diameter wires were fabricated with excellent structures and only minor surface silicide formation on the wires. Several impact strength values were considerably over those expected for monolithic Si_3N_4. The improved properties were attributed to increased fracture surface energy associated with plasticity resulting from pull out of the wires. Severe silicide reactions prevented successful fabrication of composites using superalloys. Other promising work in this area and techniques for limiting metal oxidation problems are discussed.

Dense Si_3N_4 was hot pressed at a 250°K lower temperature using a 10 Kpsi pressure compared with the usual 4 Kpsi. This was important in minimizing interactions with wire reinforcements. It was also found that acceptable densities could be achieved at normal temperature and pressure with as little as 1/8 w/o MgO densification aid. The low MgO concentration Si_3N_4 had the highest high temperature impact strengths, highest high temperature short time bend strengths, but inferior stress rupture properties. The latter result was attributed to the effect of concentration of a $MgSiO_3$ grain boundary phase on creep rate and accommodation prior to the onset of cavitation. The low MgO contents resulted in lower strengths at room temperature apparently as a result of higher residual porosity.

Near optimum fabrication conditions were established for SiC powders from three vendors. The use of 10 Kpsi hot pressing pressure significantly enhanced densification kinetics allowing for the achievement of a 99+% dense 6 μm grain size billet with an impact strength of a factor of 6 over previous work and equivalent to monolithic Si_3N_4. This same material had short time bend strengths of 72 Kpsi at 70°F and 2000°F. Strength fell to 55 Ksi at 2400°F which suggested that larger grain size material (18 μm) with a nearly constant 50 Kpsi bend strength with temperature to 3200°F may prove desirable for stress rupture and creep considerations.

II. INTRODUCTION

Higher gas turbine inlet temperatures will improve engine efficiency which means specific fuel and air consumption will decrease with power per unit weight increasing. These incentives as well as reduced gas pollution problems lend considerable inducement toward developing materials that can perform efficiently in a higher temperature turbine environment both in the vane and blade configuration. Materials for the vane application with its lower mechanical stress requirements are expected to be available first. Preliminary testing at a number of facilities indicate that SiC and Si_3N_4 base materials have the necessary oxidation resistance, thermal shock resistance, strength, stress rupture life and chemical stability for consideration. An initial program conducted at Avco(ref. 1) found that Si_3N_4 appears to be superior in thermal shock resistance and strength, whereas SiC has better oxidation resistance and stress rupture strength. Low impact resistance has limited a more general application of these materials to advanced turbine concepts. Two prior programs have dealt with composite approaches to overcome this limitation. A SiC composite containing 5-25 v/o chopped C fibers exhibited improved impact strengths over an unreinforced matrix. In the Si_3N_4 system, the greatest gains were made through the use of α Si_3N_4 powder which gave high bend strengths together with high impact strengths. The impact strength of Si_3N_4 was further increased by a factor of three with the application of a β-spodumene, lithium aluminum silicate coating. Several Si_3N_4/metal wire composite structures had promising microstructures which suggested that, with processing improvements, useful gains in impact strength may be realized.

This program followed several of the demonstrated promising approaches toward raising the mechanical impact resistance of SiC and Si_3N_4 base systems. One phase of the program dealt with improving the microstructure and strength of the base matrices. A second effort centered on forming a ductile metal/Si_3N_4 composite by the incorporation of wires via hot pressing or infiltration of a porous Si_3N_4 skeleton. Improvement of the β-spodumene coating to Si_3N_4 received additional attention in this program.

III. FABRICATION

A. Monolithic Silicon Nitride, Silicon Oxynitride, and Silicon Carbide

1. Silicon Nitride

a. Powder

Controlled phase grade (CPG) Si_3N_4 powder was purchased from Advanced Materials Engineering Ltd. This grade will hereafter be designated as CPG. The salient chemical and physical properties of the CPG powder is listed in Table I. The crystallite morphologies of the CPG powder is illustrated in Figure 1. There appears to be two distinct particle sizes in the powder. The rod shaped crystals undergo a significant increase in the diameter to length ratio, which suggests that these are precursors of the more blocky crystallites.

Powder was prepared for pressing by making densification aid additions of from 1/8% to 4% MgO. The fine particulate MgO was added by

TABLE I

Controlled Phase Grade

Si_3N_4 Powder Properties

Grade	Vendor Reported Impurity Concentration	Semi-Quantitative Phase Concentration (X-ray)			Particle Size (microns)
		α Si_3N_4	β Si_3N_4	Other	
Controlled Phase	< 2%	85%	15%	Trace FeSi	.75

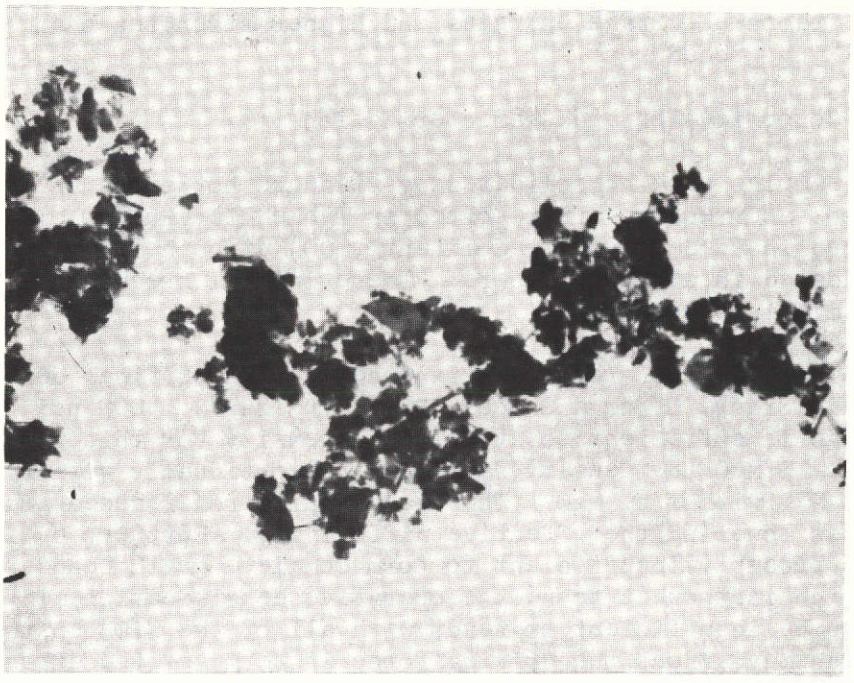

73053 (a) 7500X

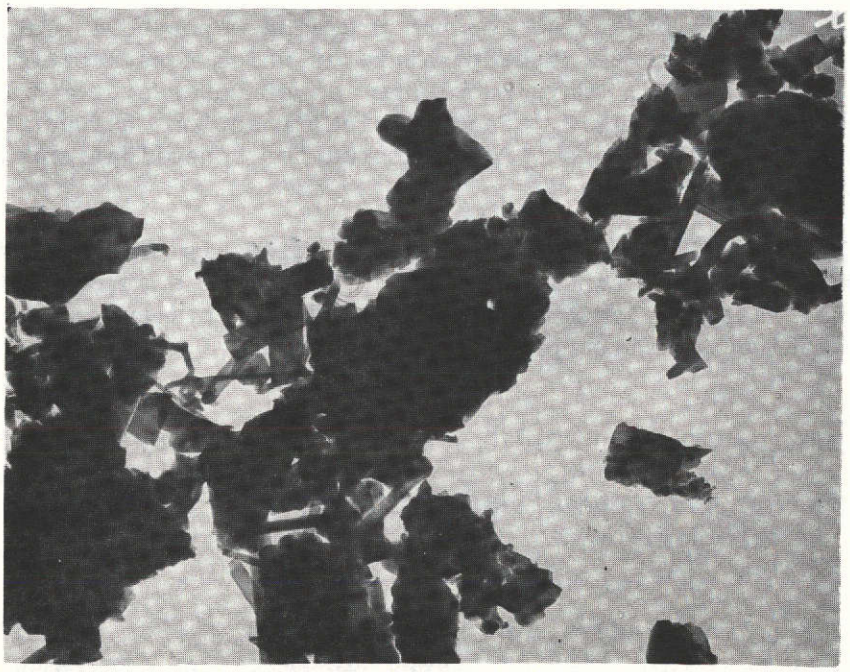

73054 (b) 30,000X

Figure 1. Crystallite Morphology for AME Controlled Phase Grade Powder.

wet milling in t-butanol using WC balls for 16 hours. This procedure was shown by Lange and Terwilliger[ref. 2] to result in hot pressed material with higher fracture surface energies and higher strengths than several alternate mixing procedures.

b. Consolidation and Characterization

Samples were consolidated by standard hot pressing techniques. The conditions and results are reported in Table II. Runs D1810 and D1835 were conducted in an ambient (predominantly CO) atmosphere while all others were consolidated in a N_2 atmosphere. These initial pressings also lacked the special milling procedure.

The effect of reduced MgO concentration on final density is illustrated in Figure 2 for a 2-hour, 2023°K (3182°F), 4000 psi pressing cycle. 1% MgO is sufficient to attain full density for this pressing cycle. Below 1% MgO the density falls off proportionally with reduced MgO reaching 97% with 1/8% MgO. This may result from reduced grain boundary film thickness lowering the effective diffusivity. Further, by 1/8% the MgO level is probably insufficient to form complete grain boundary wetting by $MgSiO_3$ which is thought to be the operative densification aid[ref. 3]. This may also be insufficient to react with all of the SiO_2 on the powder surface, which may affect the driving force in terms of the effective surface energies as well as the kinetics. This line of reasoning was employed in designing the experiment whose main purpose was to determine whether or not improved high temperature properties could be obtained by having incomplete grain boundary wetting.

The second objective for the pressing reported in Table I was to determine the lower level of temperature at which reasonable densities ($>95\%$) could be obtained. This knowledge was of interest for the composite work reported in Section III.C. since chemical reactions between Si_3N_4 and candidate reinforcement metals were predicted for consolidation above 1873°K [ref. 1].

Figure 3 illustrates the interrelationship of temperature and consolidation pressure on final density. Pressure is a strong driving force for densification as might be expected for a covalently bonded compound. This investigation proved the potential of pressing composites at 1500°C.

Samples D1851 and D1870 were characterized by X-ray diffraction and standard microstructure analysis. Both samples were predominantly β -Si_3N_4; however, D1870 contained a minor fraction of Si_2N_2O. In addition, both samples contained minor diffraction lines which were thought to be FeSi, WC, and WSi_2.

The polished and etched structure of Si_3N_4 + 1 w/o MgO, D1851, is shown in Figure 4. The high density, 3.18 gm/cc, is confirmed by the micrographs. Also shown are the two or three trace phases FeSi, WC, and WSi_2. The FeSi phase is present in the starting material and is common to most hot pressed Si_3N_4. A lineal analysis of Figure 4b established the concentration of all second phases to be between 1-2 vol. %. It is not known how this phase affects mechanical properties; however, it is the

TABLE II

Silicon Nitride and Oxynitride Fabrication Conditions and Results

Run No.	Material	Additive	Temp. °F	Temp. °K	Pressure psi	Pressure MN/m^2	Time min.	Density gm/cc	Density $Kg/m^3 \times 10^3$	Grain Size μm
D1810	AME - Si_3N_4 CPG	½ w/o MgO	3236	2053	4000	27.5	120	3.15	3.15	-
D1835	AME - Si_3N_4 CPG	4% MgO	3236	2053	2000	13.8	120	3.19	3.19	-
D1851	AME - Si_3N_4 CPG	1 w/o MgO	3182	2023	4000	27.5	120	3.18	3.18	0.78
1670	AME - Si_3N_4 CPG	4 w/o MgO	2570	1683	15000	103.1	60	1.98	1.98	-
D1864	AME - Si_3N_4 CPG	1 w/o MgO	3182	2023	4000	27.5	120	3.19	3.19	-
D1870	AME - Si_3N_4 CPG	¼ w/o MgO	3182	2023	4000	27.5	120	3.12	3.12	0.95
D1872	AME - Si_3N_4 CPG	½ w/o MgO	3182	2023	4000	27.5	120	3.14	3.14	-
1672	AME - Si_3N_4 CPG	4 w/o MgO	2822	1823	12000	82.6	120	3.14	3.14	-
1673	AME - Si_3N_4 CPG	4 w/o MgO	2732	1773	12000	82.6	120	3.13	3.13	-
D1909	AME - Si_3N_4 CPG	1/8 w/o MgO	3182	2023	4000	27.5	120	3.09	3.09	-
993	AME - Si_3N_4 CPG	¼ w/o MgO	3182	2023	3000	20.6	120	3.07	3.07	-
D1873	Norton Si_2N_2O	5 w/o MgO	3182	2023	4000	27.5	120	2.89	2.89	-

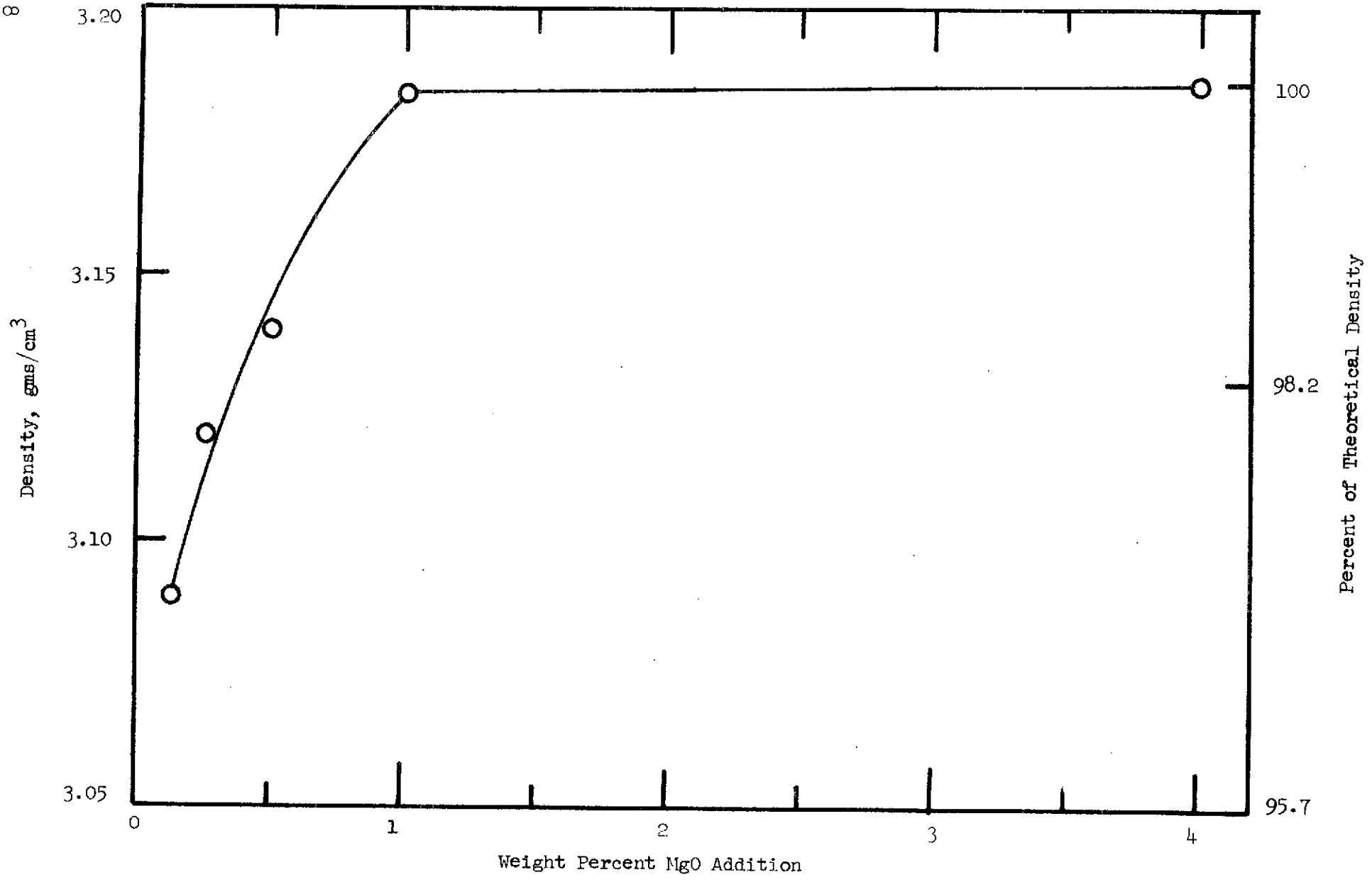

Figure 2. Effect of MgO on Final Si_3N_4 Density for a Constant 2023°K, 4000 psi, 2 hour Pressing Cycle.

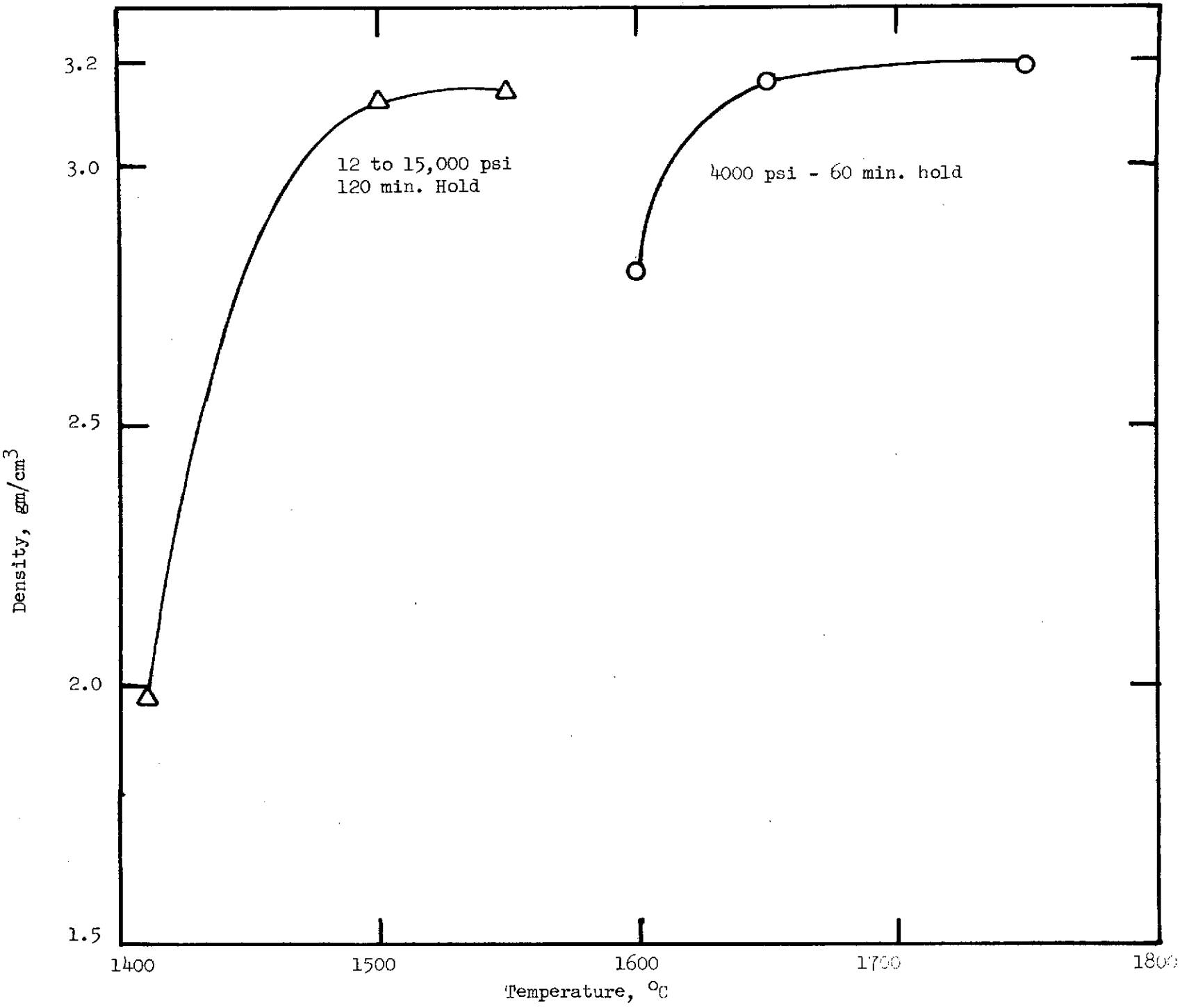

Figure 3. Effect of Temperature on Final Si_3N_4 (+ 4 w/o MgO) Density for Two Different Pressure Regimes.

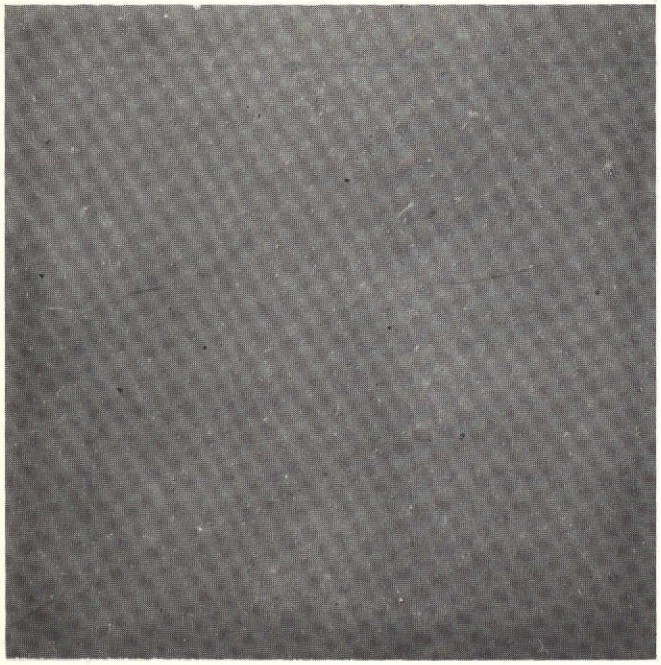

5701-1 (a) 100X

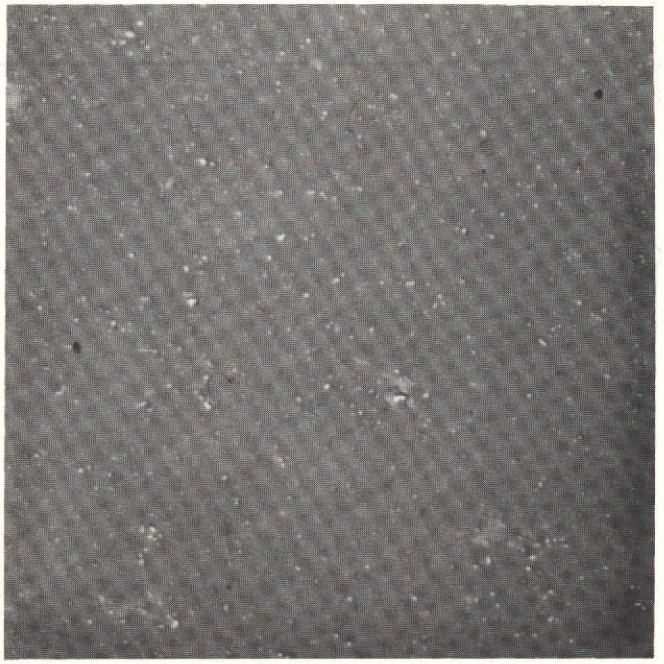

5701-2 (b) 500X

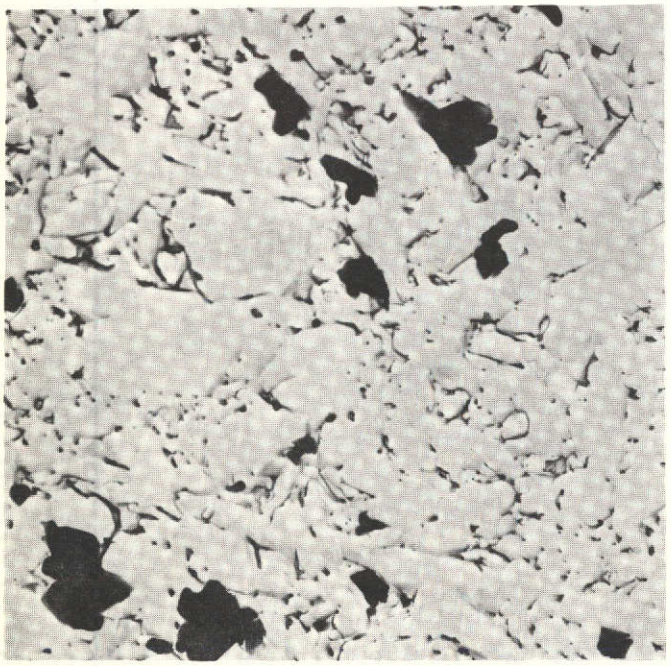

72528 (c) 7500X

72529 (d) 30,000X

Figure 4. Si_3N_4 + 1 wt. % MgO, D1851, Showing Details of Polished and Etched Structure; the grain size is 0.78 microns.

This page is reproduced at the back of the report by a different reproduction method to provide better detail.

general view that it is detrimental. The particle size is from 1-3 μm and the high temperature mechanical properties of an iron silicide phase are not expected to be as good as Si_3N_4 or the grain boundary phase controlling high temperature properties. The tungsten phases are a result of contamination from the balls in milling. Again, this is not desirable and a series of controlled milling experiments could probably find an optimum level of milling to minimize W pick up and gain the benefits of milling. The average matrix grain size is 0.78 μm; however, grains up to 2 μm are noted. The only noticable difference in the Si_3N_4 billets having lower MgO concentrations was the increased porosity. The grain size of Si_3N_4 + ¼% MgO, D1870, was 0.95 μm, for example.

2. Silicon Oxynitride

Silicon oxynitride powder was obtained from Norton Company. The particle size was about 2 μm and consisted mainly of Si_2N_2O. In addition, about 8 wt. % β-Si_3N_4 and 3 wt. % α-Si_3N_4 as well as a trace of a phase best identified as FeSi were found. The pressing conducted with this powder employed a 5 wt. % MgO addition and was consolidated under the conditions outlined in Table II. The consolidated billet relative density was 93.8% assuming a theoretical density of 3.1 gm/cc.

X-ray examination of the final product gave Si_2N_2O as the major phase. About 12 wt. % β-Si_3N_4 was found, suggesting that the α had transformed into β-Si_3N_4. A trace of WC was detected which undoubtedly is a contaminant from the milling operation. The polished microstructure, Figure 5, confirms the moderately high density and multiphase nature of the structure.

3. Silicon Carbide

a. Powder

Three grades of silicon carbide powder were obtained from Carborundum Co., one from Ferro Co., and one from PPG Industries. Coulter Counter analyses of these powders are reported in Figure 6. Water sedimentation techniques were employed to separate a 30% fraction of fines from the Carbo. 1500 grit powder. The Ferro 2600 grit powder actually turned out to be intermediate in particle size to the 1200 and 1500 grit Carborundum powder. Water sedimentation resulted in a very small difference in average particle size, but effectively removed the large particle size tail from the distribution of sizes. The PPG powder was too fine for Coulter Counter analysis. The size and morphology of the PPG powder is illustrated in Figure 7. The largest particles are about 1 μm with 0.4 μm an approximate average size.

The powders were analyzed by X-ray diffraction. These results, reported in Table III, did not detect impurity phases. The Carborundum and Ferro powders were αSiC, while the PPG Industries' powder was the low temperature form, βSiC. Also noted in Table III are supplier impurity analyses. The Carborundum powder is apparently purer than the Ferro powder. It is not possible to comment on the relative ranking of the PPG powder, since the common cations were not sought. This particular PPG powder lot employed did contain SiC grains and agglomerates up to 200 μm in diameter. These were largely eliminated in subsequent lots.

5764-3 500X

Figure 5. Si_2N_2O, D1873, Showing β Si_3N_4 and WC in Addition to Matrix Phase.

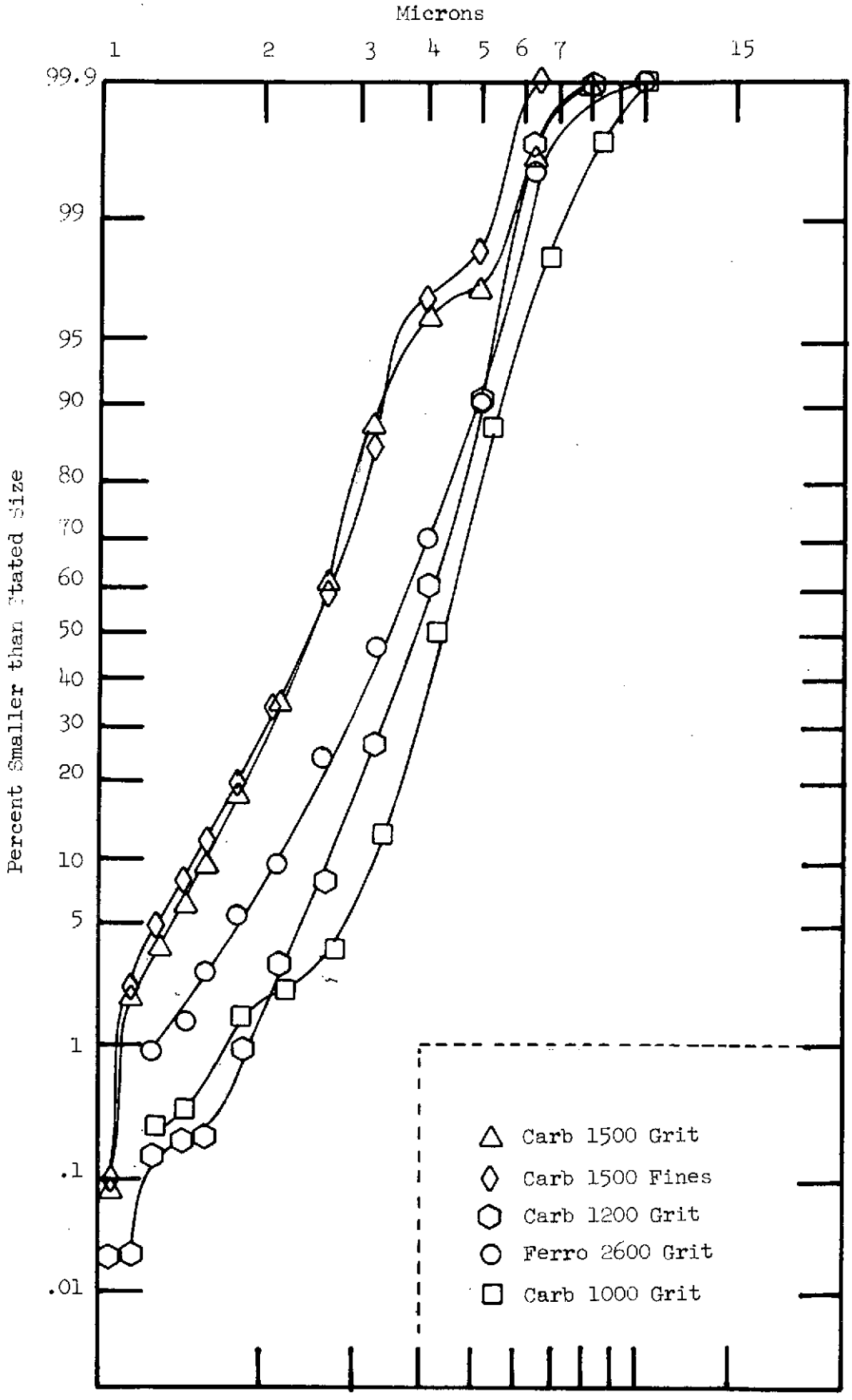

Figure 6. Crystallite Size Distributions for Four SiC Powders and Separated Fines.

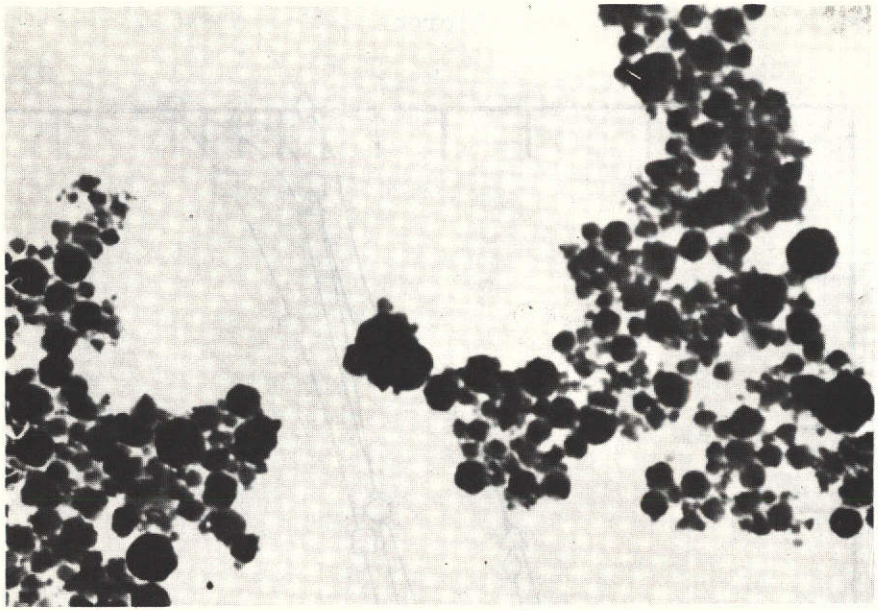

72428 7500X

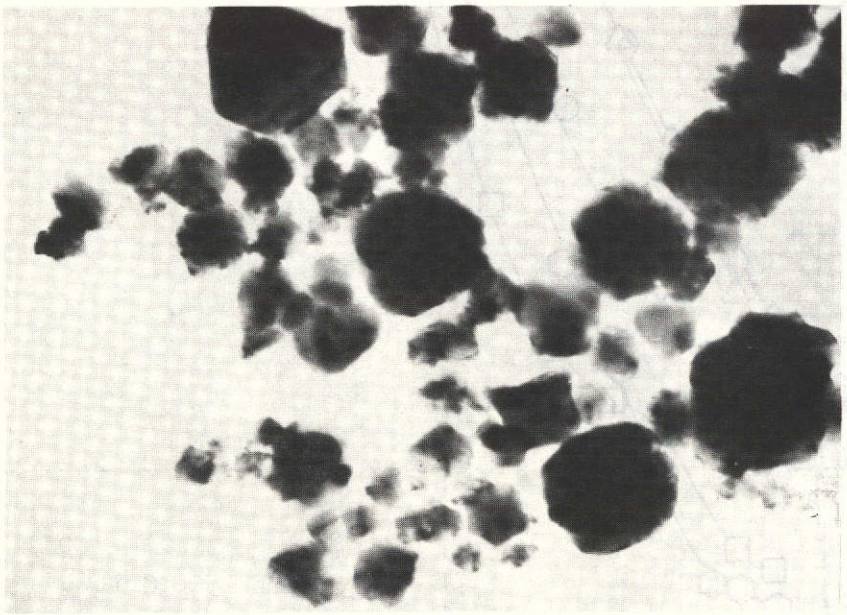

72430 30,000X

Figure 7. Crystallite Size of Pittsburg Plate Glass SiC Powder.

TABLE III

Characteristics of SiC Powders

Supplier	Phase Analysis	Impurities
Carborundum	α SiC	0.02% Si 0.86% SiO_2
Ferro	α SiC	0.3% Si 0.1% Al 0.48% SiO_2
PPG Industries	β SiC	0.01% Cl

b. Consolidation and Characterization

The SiC pressing conditions and results are listed in Table IV. Most of the billets were pressed at 4 Kpsi as 3-4 Kpsi is practical for the fabrication of large size billets. Several runs were conducted at 10 Kpsi and 2223°K compared to the 2413° - 2513°K employed for the 4 Kpsi pressings. Figure 8 illustrates the interrelationships of process parameters at 4 Kpsi pressing pressure and final microstructure for the 5 powders. The series showed that it was difficult to end up with < 20 μm grain size using the Carborundum or Ferro powder. There were negligible differences among the three grades of Carborundum powder. The use of separated fines did not result in increased densification kinetics or decreased final grain size. There may have been a benefit in reduced incidence of secondary grain growth, but this was not proven. Pressing the 1200 grit Carborundum powder at 2473°K for 60 minutes results in a 13 μm grain size (corrected by the geometrical factor of 1.5) and 98.3% of theoretical density which is judged to be an excellent compromise between grain growth and density. The microstructure of billet D1886 processed by this cycle is shown in Figure 9. The concentration of Al_2O_3 and C densification aids was varied between 1-3 wt. %. Measurable second phase was noted for 3 wt. %, while 1 wt. % gave inadequate densification. The $1\frac{1}{2}$ wt. % level was chosen as near optimum with only a trace of second phase apparent.

The Ferro SiC powder could not be fully densified employing $1\frac{1}{2}$ wt. % additions of Al_2O_3 and C, together with process cycles that were considered severe judging by experience with the Carborundum powder. However, increasing the concentration of additives to 3 wt. % resulted in a 99.5% dense, 16 μm grain size billet, D1890, after a 2513°K - 4 Kpsi - 200 min. cycle. This structure is shown in Figure 10. Since the starting particle size was about the same as the Carborundum powder, the requirement for increased densification aid must be related to overall chemistry. The subtleties of this interaction are not understood.

The PPG Industries' powder densified readily with $1\frac{1}{2}$% of the Al_2O_3 and C densification aids in as little as 15 minutes at 2413°K and 4000 psi. However, the use of 3% Al_2O_3 alone or no additive resulted in only 83 - 86% density. Billet D1906 pressed with 1 wt. % B reached 96% density after only 60 minutes at 2293°K. Figure 11 illustrates the etched

TABLE IV

Silicon Carbide Fabrication Conditions and Results

Run No.	Material	Additive	Temp. °F	Temp. °K	Pressure psi	Pressure MN/m^2	Time min.	Density gm/cc	Density $Kg/m^3 \times 10^3$	Grain Size μm
D1763	Carb. 1000 G SiC	3 w/o Al_2O_3 3 w/o C	4064	2513	4000	27.5	200	3.15	3.15	-
D1792	PPG SiC	3 w/o Al_2O_3	3938	2443	4000	27.5	180	2.67	2.67	-
D1800	Carb. 1000 G SiC	1½ w/o Al_2O_3 1½ w/o C	4064	2513	4000	27.5	200	3.17	3.17	23
D1818	Carb. 1000 G SiC	1½ w/o Al_2O_3 1½ w/o C	3884	2413	4000	27.5	180	3.18	3.18	19
D1819	Carb. 1000 G SiC	1½ w/o Al_2O_3 1½ w/o C	4064	2513	4000	27.5	60	3.14	3.14	18
D1821	Ferro 2600 G SiC	1½ w/o Al_2O_3 1½ w/o C	3884	2413	4000	27.5	90	2.52	2.52	-
D1823	PPG SiC	1½ w/o Al_2O_3 1½ w/o C	3884	2413	4000	27.5	40	3.19	3.19	5
D1829	Carb. 1200 G SiC	1½ w/o Al_2O_3 1½ w/o C	3884	2413	4000	27.5	180	3.16	3.16	23
D1837	Carb. 1500 G SiC	1½ w/o Al_2O_3 1½ w/o C	3884	2413	4000	27.5	180	3.17	3.17	21
D1856	Ferro 2600 G SiC	1½ w/o Al_2O_3 1½ w/o C	4064	2513	4000	27.5	60	2.66	2.66	-
D1860	Carb. 1500 G SiC	1½ w/o Al_2O_3 1½ w/o C	3884	2413	4000	27.5	115	3.11	3.11	10
D1861	Carb. 1000 G SiC	1 w/o Al_2O_3 1 w/o C	3884	2413	4000	27.5	180	2.98	2.98	18

TABLE IV cont.

Run No.	Material	Additive	Temp. °F	Temp. °K	Pressure psi	Pressure MN/m^2	Time min.	Density gm/cc	Density $Kg/m^3 \times 10^3$	Grain Size μm
D1863	Carb. 1500 GF SiC	1½ w/o Al_2O_3 1½ w/o C	3884	2413	4000	27.5	115	3.16	3.16	-
D1883	Carb. 1000 G SiC	1 w/o B	3668	2293	4000	27.5	60	3.00	3.00	-
D1886	Carb. 1200 G SiC	1½ w/o Al_2O_3 1½ w/o C	3992	2473	4000	27.5	60	3.15	3.15	13
D1888	PPG - SiC	-	4064	2513	4000	27.5	160	2.75	2.75	-
D1890	Ferro 2600 G SiC	3 w/o Al_2O_3 3 w/o C	4064	2513	4000	27.5	200	3.20	3.20	16
D1906	PPG - SiC	1 w/o B	3668	2293	4000	27.5	60	3.08	3.08	4 x 35
D1908	PPG - SiC	1½ w/o Al_2O_3 1½ w/o C	3884	2413	4000	27.5	15	3.21	3.21	3 x 30
R2019	PPG - SiC	1 w/o B 1 w/o C	3542	2223	10,000	68.8	60	3.21	3.21	5 x 60
R2020	Carb. 1500 G SiC	1½ w/o Al_2O_3 1½ w/o C	3542	2223	10,000	68.8	60	3.23	3.23	7
996	PPG - SiC	1½ w/o Al_2O_3 1½ w/o C	3632	2273	3000	20.6	30	3.14	3.14	5

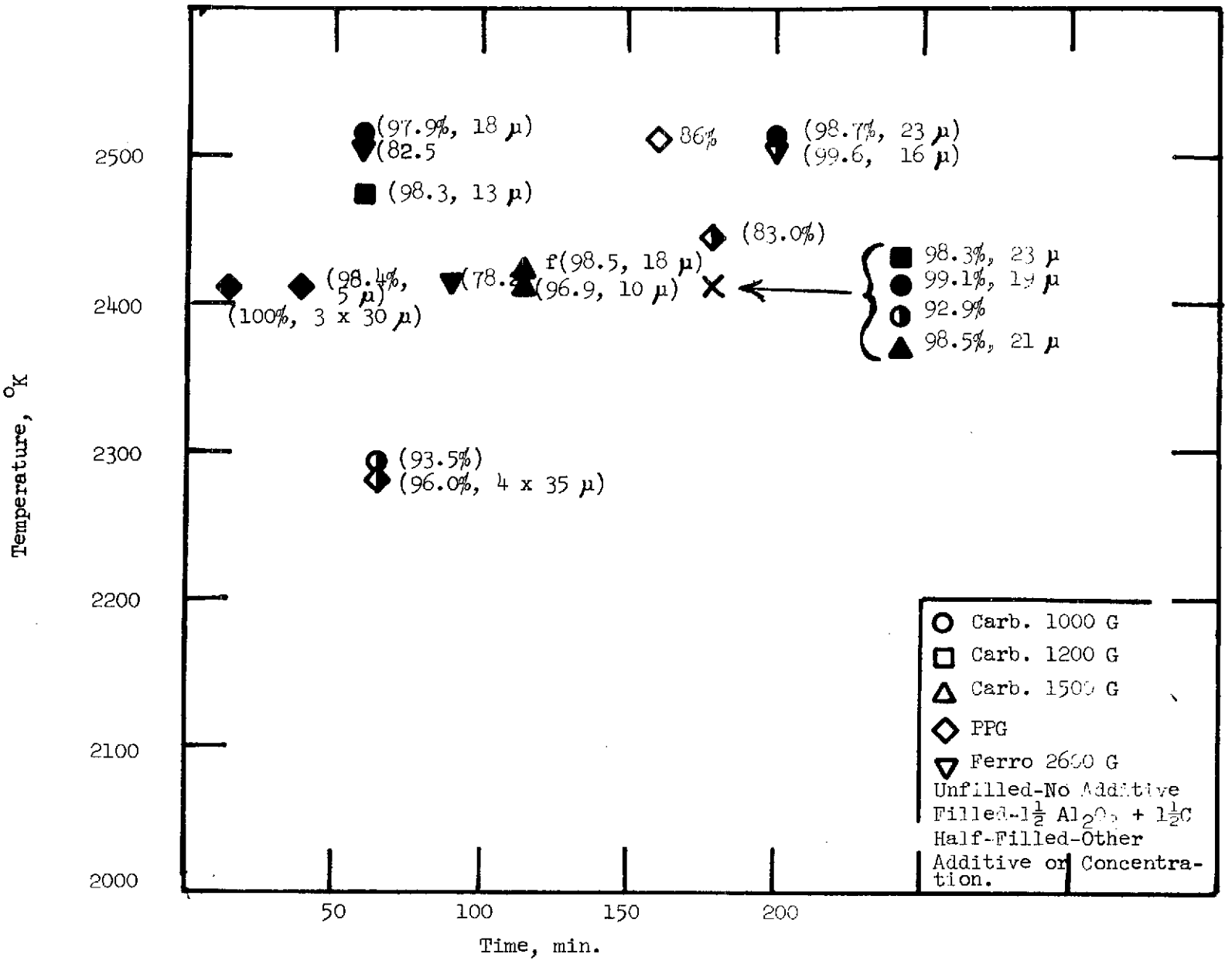

Figure 8. **Processing-Microstructure-Powder Relationships for SiC Pressed at 4000 psi.**

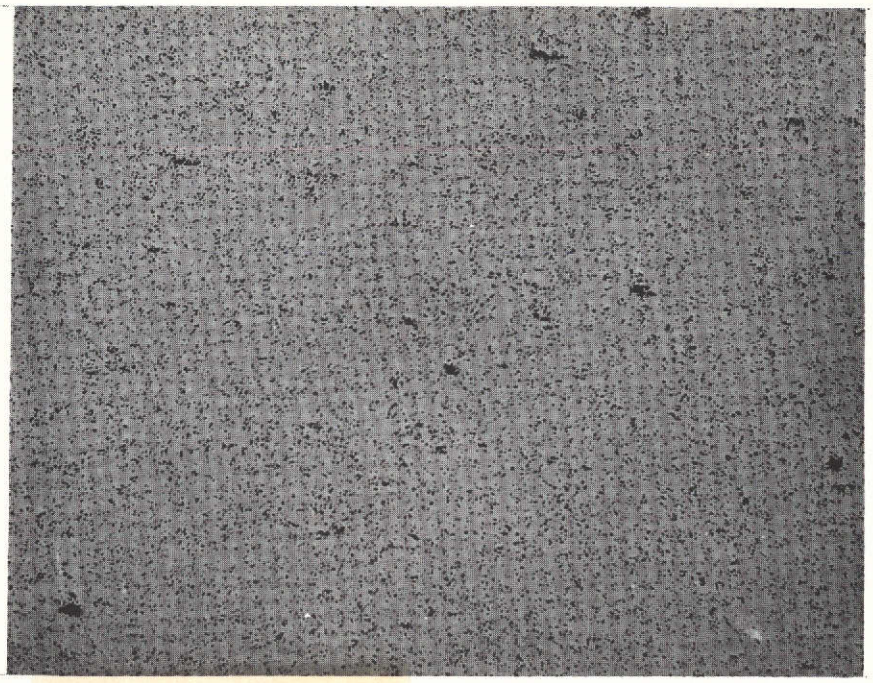

5764-6 (a) 100X

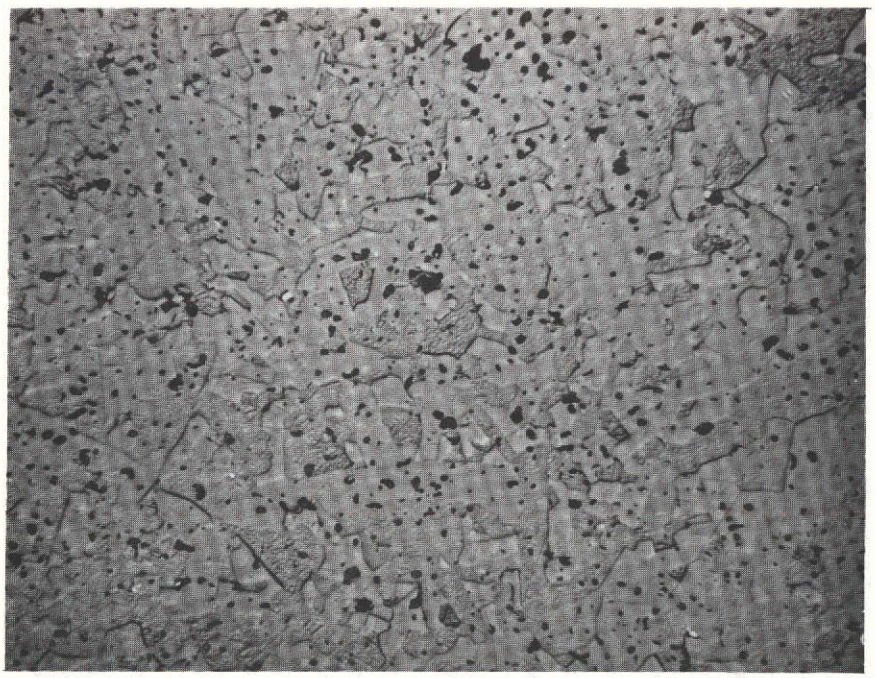

5764-8 (b) 500X

Figure 9. Microstructure of SiC billet D1886 Pressed at 2200°C - 4000 psi - 60 min. Using 1200 Grit Carborundum Powder (a) As-Polished, and (b) Etched.

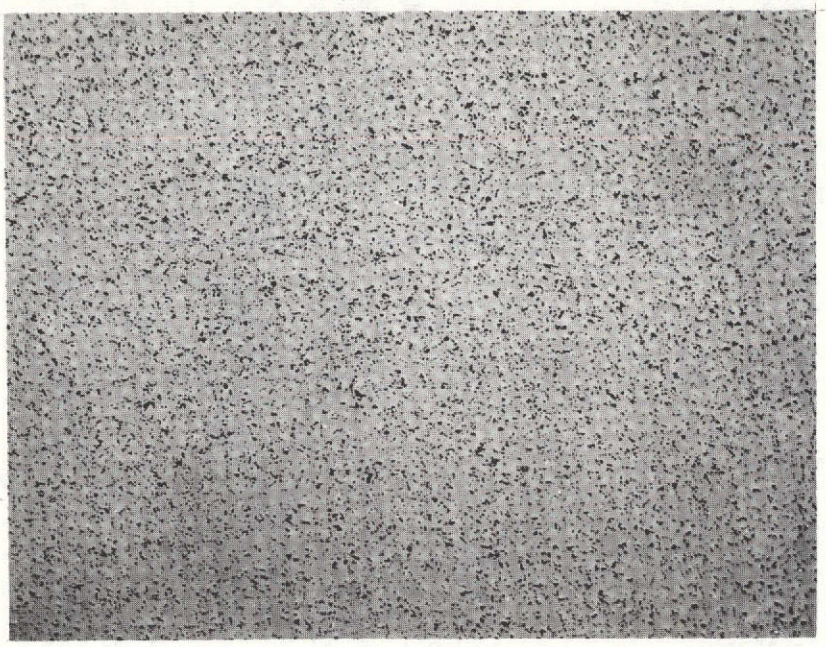

5764-9 (a) 100X

This page is reproduced at the back of the report by a different reproduction method to provide better detail.

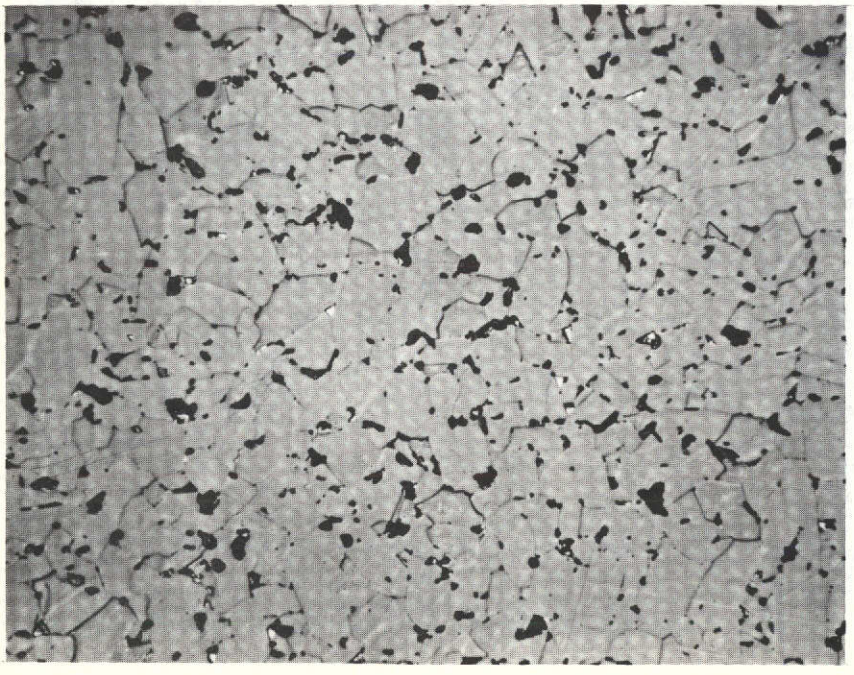

5764-11 (b) 500X

Figure 10. Microstructure of SiC billet D1890 pressed at 2240°C - 4000 psi - 200 min. using 2600 grit Ferro powder (a) as-polished, and (b) etched.

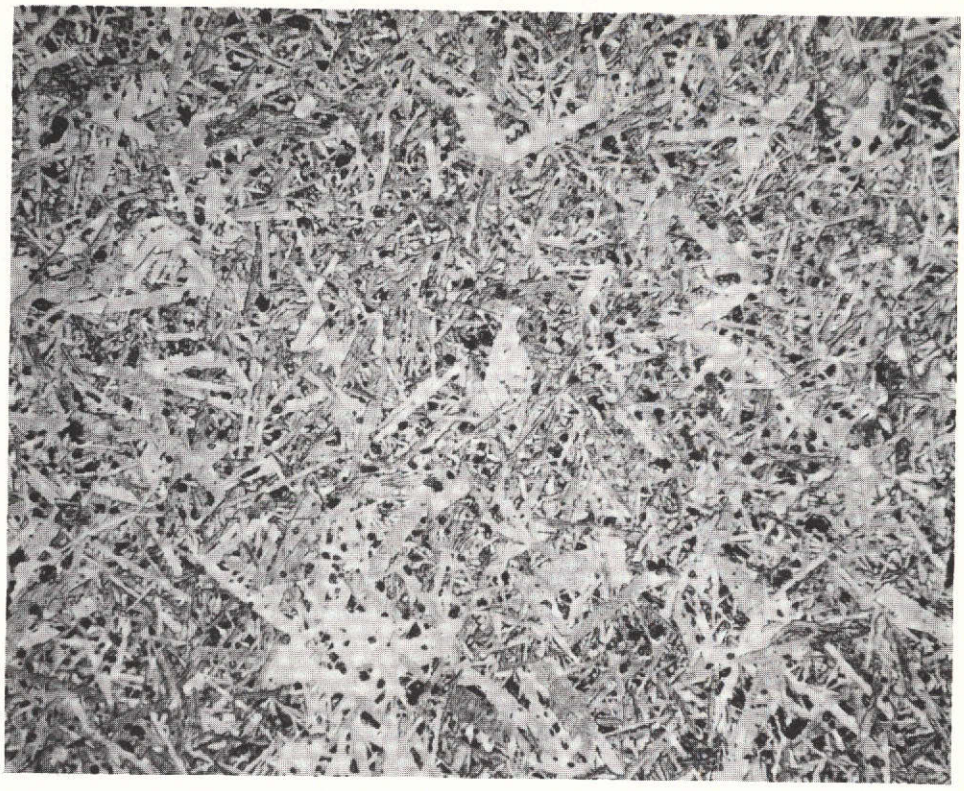

5783-3 500X

Figure 11. Etched Structure of SiC Billet D1906 Pressed at 2020°C - 4000 psi - 60 mins. with PPG Industries' Powder Plus 1 wt. % B.

This page is reproduced at the back of the report by a different reproduction method to provide better detail.

structure of this billet, demonstrating the occurrence of marked secondary grain growth. This phenomena has also been observed by Prochazka(ref. 4) using the B addition. He found that this structure could be suppressed by the addition of C. He also noted that the elongated grains were α SiC, whereas the equiaxed structure was β SiC, indicating the phase transformation was involved in the onset of secondary grain growth. Use of the standard $1\frac{1}{2}$ wt. % Al_2O_3 + C additions to PPG Industries' powder resulted in two billets (D1823 and 996) having slightly tabular 5 μm grains, for example D1823 (Figure 12). All of the others had some exaggerated grain growth, although often in a matrix of fine grains. X-ray examination showed both billets, D1906 and D1823 (Figures 11 and 12) to be α SiC in contrast to the results of Prochazka(ref. 4). This proves that the transition from β to α SiC does not necessarily result in secondary growth; thus, the remaining problem is not one of controlling the phase transition, but learning how to control secondary growth. Several of the billets showed isolated large grains which could be the large grains noted in the powder. This powder shows great promise for the achievement of dense fine grained SiC; however, additional work is required both in powder manufacture and process control.

Pressure is an effective processing variable for SiC as well as for Si_3N_4 as discussed earlier. Nearly full density (3.23 gm/cc) was achieved in pressing R2020 employing Carborundum 1500 grit SiC powder plus $1\frac{1}{2}$ Al_2O_3 and $1\frac{1}{2}$ C after 60 min. at 2223°K and 10 Kpsi. None of the other pressing conditions gave as high a density. The grain size was only 6 um, as shown in Figure 13. This compares with 13 μm for the next smallest grain size using this powder where 98.3% density was reached (billet D1886). This microstructure was considered highly desirable, but unfortunately 10 Kpsi pressing conditions are difficult to achieve for diameters larger than about 3 inches.

C. Composites

1. Fabricated by Hot Pressing

a. Systems

All of the composites fabricated in this program were Si_3N_4 base. The reinforcement phases were for the most part metal wires which, in theory, would provide marked increase in fracture surface energy through plastic processes and/or wire pull-out energy. The problem, as with any composite, was to fabricate a body with a high quality matrix while at the same time incorporating the reinforcement without degradation of its properties.

A previous program(ref. 5) had taught that Mo and Re could be processed with Si_3N_4 at 1973°K with limited reactions. The process objective was to further limit these reactions by lowering the pressing temperature without seriously degrading matrix density. In addition, a series of runs were made with superalloy wires to explore the feasibility of such systems. Finally, several runs were made with Ta wire reinforcement as Brennan and Decrescente(ref. 6) had noted some success with this system.

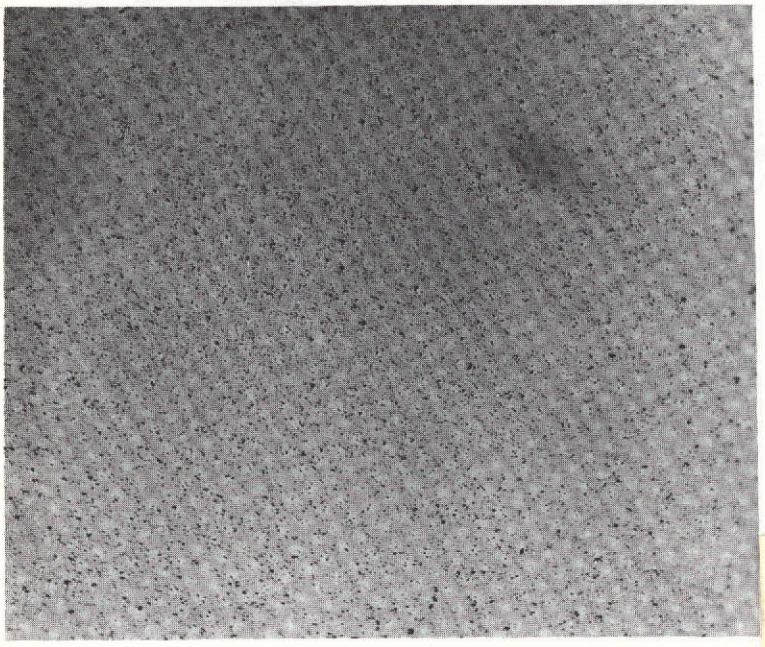

5684-1 (a) 100X

5684-3 (b) 500X

72526 (c) 1500X

Figure 12. Microstructure of SiC Billet D1823 Pressed at 2140°C - 4000 psi - 40 min. using PPG Industries' Powder (a) As-polished, (b) Etched, and (c) Replica of Fracture Surface.

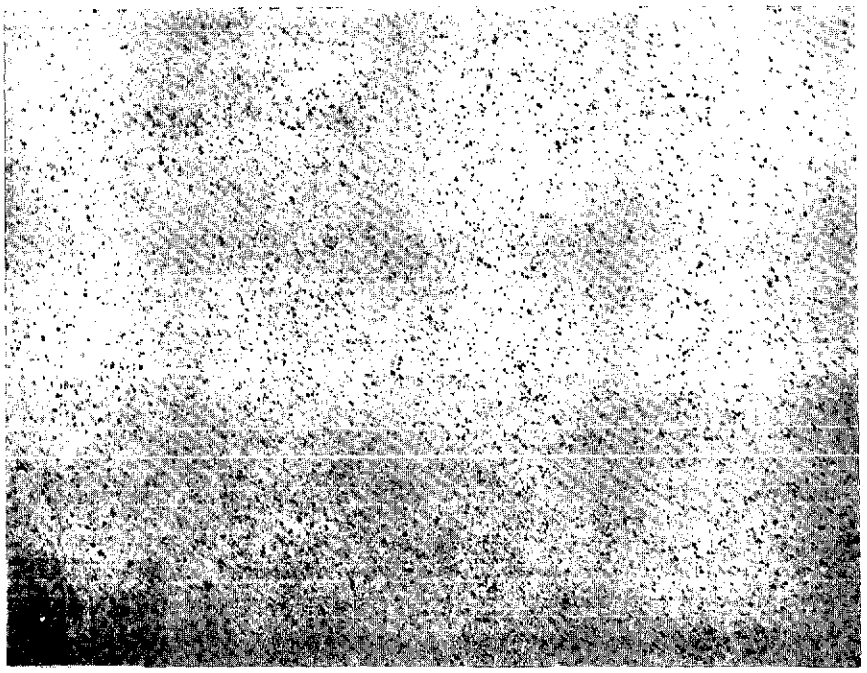

5789-1 (a) 100X

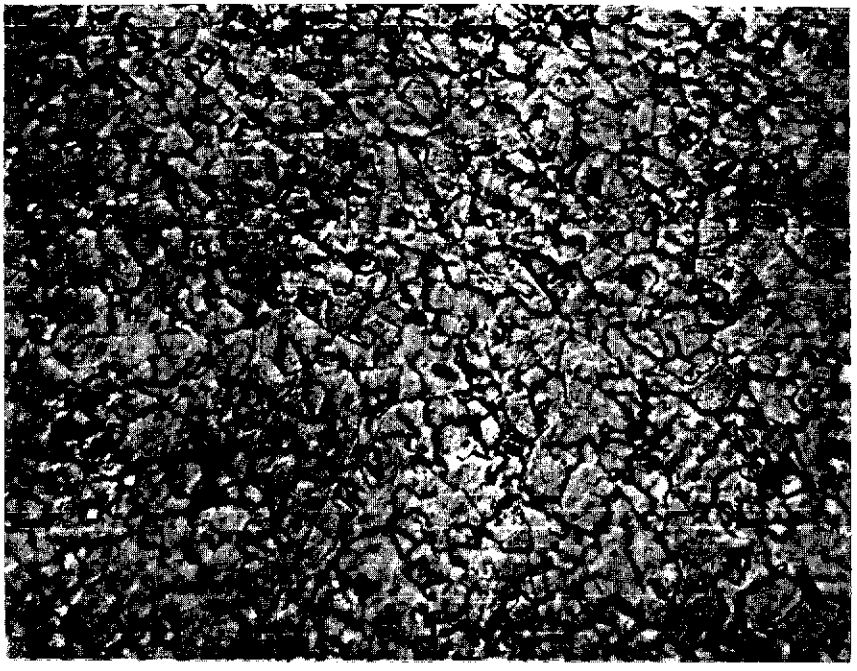

5789-2 (b) 750X

Figure 13. Microstructure of SiC Billet 2020 Pressed at 1950°C - 10,000 psi - 60 mins. Using Carborundum 1500 Grit SiC Powder (a) As-Polished, and (b) Etched.

This page is reproduced at the back of the report by a different reproduction method to provide better detail.

b. Consolidation and Characterization

Most of the billets were fabricated with aligned continuous wires. The wires, ranging from 0.005 to 0.020 inch diameter, were wound on a 54-inch circumference drum winder using a mylar substrate and spacing twice the wire diameter. The wires were sprayed with isobutyl methacrylate to hold the wire alignment, cut into 3-inch diameter discs, and stacked into the pressing die with the appropriate quantity of Si_3N_4 + 4 w/o MgO powder between layers. The plastics used were expected to volatilize during heating (this system was optimized in B/Al composite fabrication studies). One billet was fabricated using chopped random Mo wires by a procedure previously described(ref. 5).

The run conditions and results are listed in Table V. Run 1894 with 0.005 inch diameter Ni20Cr wires was typical of the runs with various superalloys. The structure shown in Figure 14 demonstrates melting and penetration of the metal into the Si_3N_4 matrix. The matrix itself appears denser than expected from the 1773°K - 4000 psi pressing conditions, and this is attributed to action of the metal itself. Knoop hardness and X-ray analysis demonstrated that most of the metal had been converted to Ni_3Si and Cr_3Si. A limited fraction of unreacted metal remained. The 72Ni23Cr5Al alloy exhibited the greatest geometry retention of the superalloys, but, with a Knoop hardness of 620 to 810 for the metal second phase, it was judged that silicide reactions were extensive.

The two Mo wire composites were pressed at 10 Kpsi and 1773°K. The microstructure of billet R2011 containing oriented 0.010 inch diameter wires is shown in Figure 15. The 4.20 gm/cc bulk density is slightly over the theoretical density of the composite, and the high matrix density was confirmed by metallography. Also apparent was a 20 μm thick circumferential zone which was given a probable identification of Si_3Mo_5 by X-ray diffraction, and a Knoop hardness of 1170 which is near the range of $MoSi_2$(ref. 7). The central zone had a Knoop hardness of 210 compared to the literature value of 240 Knoop for annealed Mo (ref. 8). The presence of elemental Mo was also confirmed by X-ray analysis. It is noteworthy that no evidence was seen for microcracking at the Si_3Mo_5 interface which must be a point of stress concentration due to thermal expansion mismatch. Thus, from a microstructure viewpoint, a fairly respectable Si_3N_4/Mo composite system was developed. The reacted layer should exhibit less and less influence over properties as wire diameter is increased. A 9" x 9" Si_3N_4/Mo composite plate was pressed (1016) with five patterns of Mo. The patterns were laid up such that NASA burner test specimens could be machined with exposed wires on one end only.

The Ta wire composite pressing R2012 was fabricated under identical conditions to those employed for the Si_3N_4/Mo composite R2011. Metallographic examination revealed extensive wire reaction, deformation, and fracture. X-ray examination of this billet showed $TaSi_2$ and TaC and no elemental Ta. The hold time was reduced to 60 minutes for composite pressing R2021 with an improvement in structure (Figure 16). Wire deformation still occurred, but an outer reaction zone appeared limited to about 20 μm. The Knoop hardness of the wire core was 810, which is high compared with a literature value of 210(ref. 9), indicating perhaps more reaction than observed metallographically. Microcracks were present at some but not

TABLE V

Fabrication Conditions and Results

Run No.	Material	Additive	Temp. °F	Temp. °K	Pressure psi	Pressure MN/m^2	Time min.	Density gm/cc	Density $Kg/m^3 \times 10^3$
D1814	AME-3	4 w/o MgO ½ w/o C 5 w/o SiC (Carbo. 1000 G)	3182	2025	4000	27.5	120	3.15	3.15
D1894	AME-4 - Si_3N_4	4 w/o MgO 13.4 v/o Ni20Cr	2732	1773	5000	34.4	120	3.20	3.20
R2010	AME-4 - Si_3N_4	4 w/o MgO 10 v/o Mo (Random)	2732	1773	7000 10,000	48.1 68.8	60 60	3.98	3.98
R2011	AME-4 - Si_3N_4	4 w/o MgO 13.7 v/o Mo (Oriented)	2732	1773	7000 10,000	48.1 68.8	60 60	4.20	4.20
R2012	AME-4 - Si_3N_4	4 w/o MgO 13.6 v/o Ta (Oriented)	2732	1773	7000 10,000	48.1 68.8	60 60	5.04	5.04
D1922	AME-4 - Si_3N_4	4 w/o MgO 14.7 v/o Kanthal (Oriented)	2642	1723	4000	27.5	135	3.20	3.20
R2021	AME-4 - Si_3N_4	4 w/o MgO 15.9 v/o Ta (Oriented)	2732	1773	10,000	68.8	60	5.30	5.30
D1924	AME-4 - Si_3N_4	4 w/o MgO 15 v/o 72 Ni23Cr5Al (Oriented)	2516	1653	5000	34.4	195	2.56	2.56
D1928	AME-4 - Si_3N_4	4 w/o MgO 10.3 v/o 72Ni23Cr5Al (Oriented)	2732	1773	4000	27.5	5	2.60	2.60

TABLE V cont.

Run No.	Material	Additive	Temp. °F	Temp. °K	Pressure psi	Pressure MN/m^2	Time min.	Density gm/cc	Density $Kg/m^3 \times 10^3$
D1933	AME-4 - Si_3N_4	4 w/o MgO 6.3 v/o Re (Oriented)	2732	1773	5000	34.4	80	3.40	3.40
D1942	AME-4 - Si_3N_4	4 w/o MgO 19 v/o Re (Oriented)	2732	1773	5000	34.4	120	3.65	3.65
1016	AME-8 - Si_3N_4	4 w/o MgO 5 patterns of Mo at ~15 v/o	2822	1823	3000	20.6	120	3.20	3.20

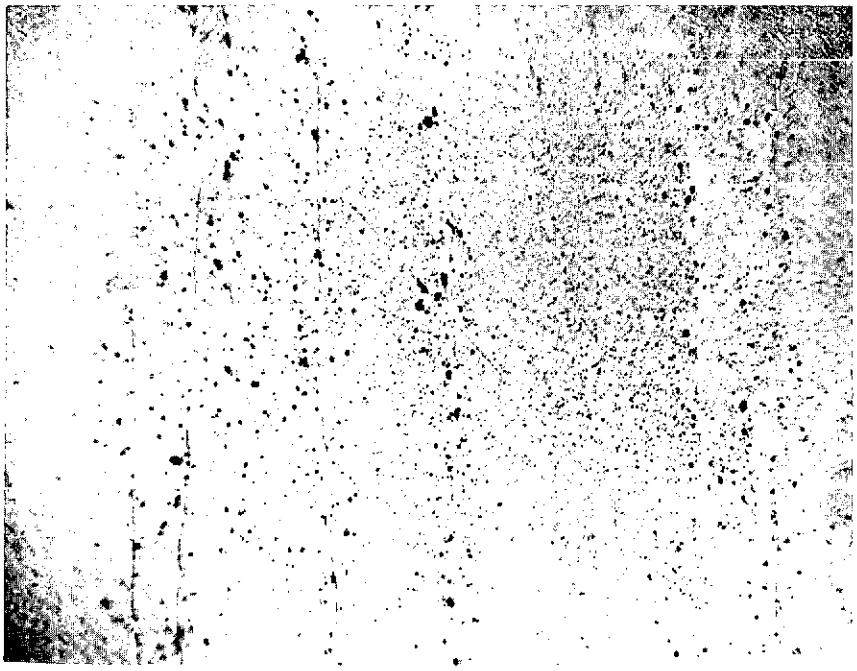

5763-1 D1894 50X

Figure 14. Microstructure of Si_3N_4/13.4 v/o Ni20Cr Wire Composite.

This page is reproduced at the back of the report by a different reproduction method to provide better detail.

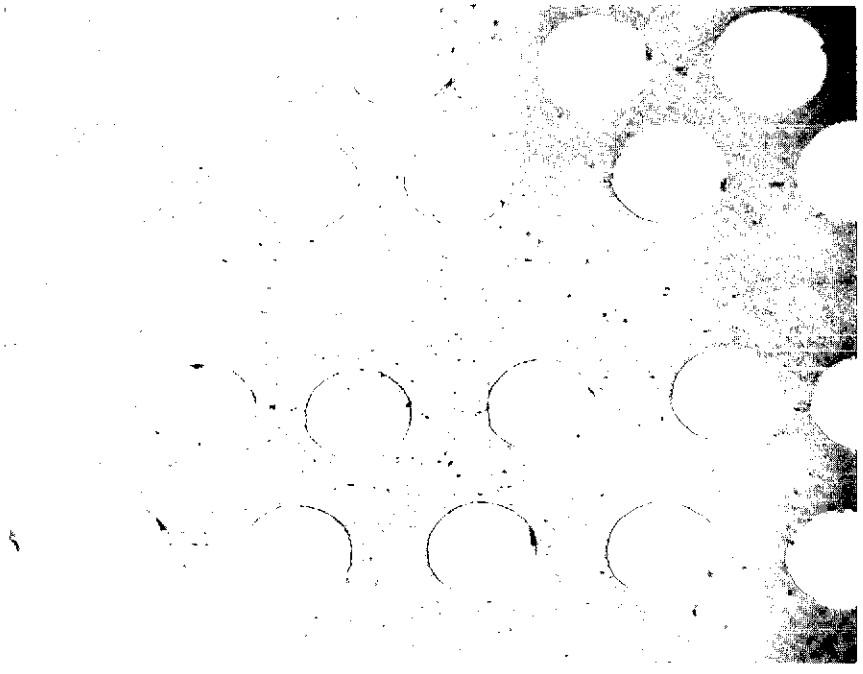

5783-12 50X

Figure 15. Microstructure of Si_3N_4/13.7 v/o Mo Wire (0.010 inch diameter) Composite, R2011.

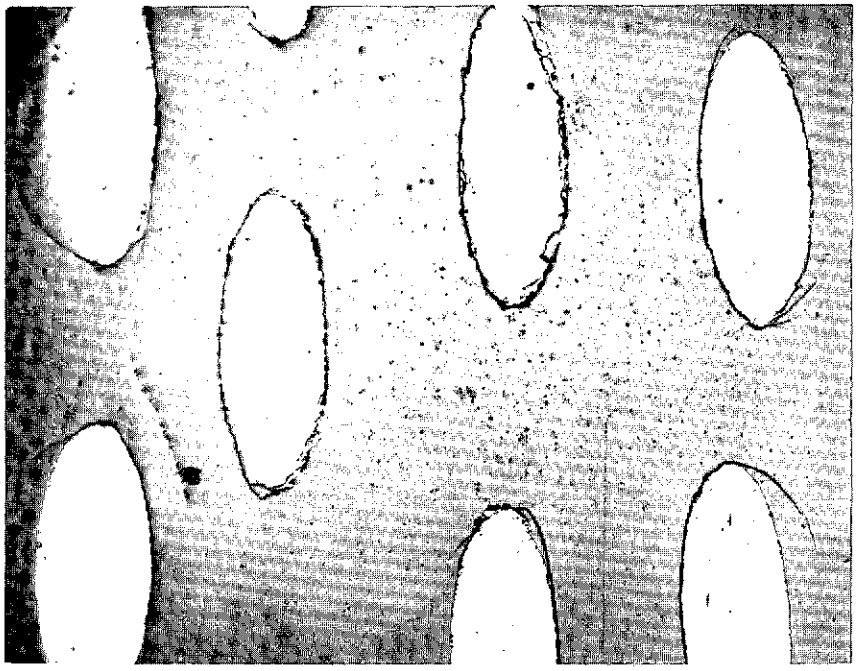

5788-2 50X

Figure 16. Microstructure of Si_3N_4/15.9 v/o Ta Wire (0.020 inch diameter) Composite, R2021.

This page is reproduced at the back of the report by a different reproduction method to provide better detail.

all of the wire/Si_3N_4 interfaces. Thus, while it appears that Ta has a higher reaction rate and greater thermal expansion mismatch than Mo, structures can be achieved that hold promise. It is also recognized that two pressings of any one combination are only enough to indicate promise.

The previous program(ref. 5) identified Re as the least reactive metal of a series of refractory metals in combination with Si_3N_4. The initial pressing, D1933, (listed in Table V) had delaminations between layers. Masking tape had been used to hold wire position on the mylar backing. It is now thought that incomplete oxidation of the tape led to the poor structure. Tape was eliminated for the second billet which solved the delamination problem. The structure of this billet shown in Figure 17 demonstrates good matrix density and a 10-20 μm interaction zone between Re and Si_3N_4. The wire had a microhardness of 455 Knoop which is intermediate between a literature value of 270 Knoop for annealed and 825 Knoop for swagged wire(ref. 8). Microcracking occurred from the elongated ends of the deformed wires and some of the wires pulled away from the matrix cracking either a segment of Si_3N_4 or Re reaction layer. Based on the microstructural evidence, the metals should be ranked Mo/Ta/Re in order of increasing thermal expansion coefficient; this is consistent with available thermal expansion data(ref. 8) which indicates Ta and Re to have similar expansions which are somewhat higher than that for Mo. The expansion and bonding character of the reaction layer may also play a role in the microcracking phenomena. This type of structure should exhibit considerable wire pull out and energy absorption associated with this process and serve as a model for examination of this behavior on impact strength.

2. Fabricated by Infiltration

Infiltration offers the possibility of incorporating a ductile superalloy into a porous SiC or Si_3N_4 matrix at markedly lower temperatures than the fabrication temperatures for either of these matrices. This lowering of temperature could be the margin required to successfully achieve a composite structure without silicide formation. Further, Ni-Cr infiltrated TiC exhibited improvements in impact strength over the matrix itself (ref. 10), and an analog structure and properties based on SiC or Si_3N_4 could have application.

Wetting studies were performed with the Ni base alloys U700, Inconel 702, NiCrAlY, Nichrome, the CO base alloy Mar M 509, and the Fe base alloy FeCrAlY on dense plaques of SiC and Si_3N_4 in vacuum between 1×10^{-3} and 2×10^{-4} torr. All of the alloys wet Si_3N_4 with a 0^o contact angle except FeCrAlY which had a 180^o contact angle. Wetting also occurred on SiC, but contact angles were somewhat higher--20^o - 65^o. Further, metallographic and X-ray studies demonstrated that all of the alloys reduced SiC to form C and complex metal silicides. The compatibility of Si_3N_4 with the Ni base alloys appeared good and little interaction with Mar M 509 was noted. However, considerable interaction occurred between Si_3N_4 and FeCrAlY at 2966^oF.

A series of seven Si_3N_4 infiltration runs were conducted under the conditions listed in Table VI. Reaction sintered Si_3N_4* and 67% dense hot pressed Si_3N_4 were chosen as matrices. The reaction sintered material was boiled in H_2O for 24 hrs. to expand the pore diameter. The runs reported

*AME Ltd.

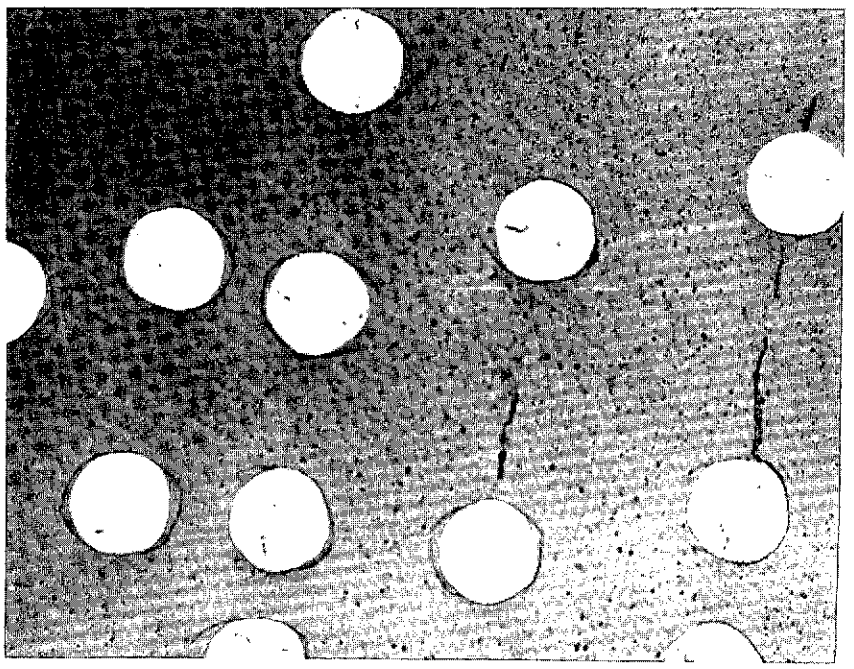

5830-7 100X

Figure 17. Microstructure of Si_3N_4/19 v/o Re Wire (0.010 inch diameter) Composite, D1942.

This page is reproduced at the back of the report by a different reproduction method to provide better detail.

TABLE VI

Infiltration Conditions and Results

Run No.	Matrix	Metal	Max. Temp. °K	Max. Temp. °F	Time Above Liquidus min.	Atmosphere	Infiltration	Matrix Condition
R-1	Reaction Sintered Si_3N_4	Inconel 702	1723	2642	90	15 torr	None	Some reaction
R-3	Reaction Sintered Si_3N_4	Inconel 702	1773	2732	90	2×10^{-3} torr	Small	Surface reaction
R-4	Reaction Sintered Si_3N_4 - boiled	Inconel 702	1723	2642	195	4 pis Ar	None	Surface reaction
R-5 a	67% Dense Si_3N_4	Inconel 702	1723	2642	225	4 psi Ar	None	No change
b	93% Dense Si_3N_4							
R-6 a	Reaction Sintered Si_3N_4 - boiled	Mar M 509	1723	2642	230	4×10^{-3} torr	Some	Some surface reaction
b	67% Dense Si_3N_4						Moderate	Surface reaction
R-7 a	Reaction Sintered Si_3N_4 - boiled	Mar M 509	1723	2642	120	4 psi Ar	Some	Surface reaction
b	67% Dense Si_3N_4						Moderate	Surface reaction
R-8 a	Reaction Sintered Si_3N_4 - boiled	Mar M 509	1548	2327	20	4 psi Ar	Some	Surface reaction
b	67% Dense Si_3N_4						Some	Surface reaction

as having been conducted in an argon atmosphere were heated to the metal liquidus temperature under vacuum between 2×10^{-6} and 1×10^{-4} torr. Once the infiltration temperature was reached, the chamber was backfilled with about 4 psi Ar as an additional driving force. The metallographic section on R-3, Figure 18, illustrates a typical result for both Inconel 702 and Mar M 509. Little true infiltration occurred, and, further, the interface exhibits evidence for interactions between phases. The high porosity in the metal and loss of vacuum at melting suggests that N was evolved from the reaction. Marked reductions in specimen size were also noted, especially in R-8 where 0.5 by 0.5 inch Si_3N_4 cross sections were reduced to 0.25 by 0.25 inch. Also noteworthy in Figure 18 is the microcrack which probably was caused by the thermal expansion mismatch.

This effort established that the infiltration method for achieving useful composites of Si_3N_4 or SiC with superalloys holds little promise. Si_3N_4/Inconel 702 was the most compatible system based on the wetting studies. However, infiltration apparently does not occur significantly faster than the reactions; and, in fact, reaction may effectively impede further penetration of unreacted metal into the pores either by generation of solid reaction products or gas evolution.

D. Coating with Lithium Aluminum Silicate

Glazed Si_3N_4 demonstrated modest improvements in impact strength (ref. 5) over control samples. The $LiAlSi_2O_6$ glaze was not considered satisfactory from the standpoint of thickness control and uniformity. In the current program a series of processing experiments on the above composition were conducted without achieving a satisfactory coating. Poorer results were achieved with the composition 2 Li 4 Al 2.5 SiO_{12}, so composition was shifted to the SiO_2 rich side; namely $LiAlSi_4O_{10}$. Excellent glaze coatings were achieved with this composition with either a dip or spray coating followed by a 120 min. 1723°K cycle in N. Figure 19 is a metallographic section of the coating on hot pressed Si_3N_4 illustrating a fully dense 20 μm amorphous layer.

IV. COMPOSITE EVALUATION

A. General

It is well recognized that SiC and Si_3N_4 and composites based on these matrices have sufficient thermal shock resistance and thermal-chemical stability for serious consideration in the turbine application. However, the mechanical shock resistance is lower than presently used nickel-base superalloy systems; e.g., B1900 has an impact strength of 108, 66, and 12 in-lbs at 2000°F, 2100°F, and 2300°F, respectively, whereas the highest impact strength measured (same conditions) for a SiC or Si_3N_4 base material was 9.5 in-lbs. (Si_3N_4). It is recognized that the impact strength measurements include the complex interaction of a number of fundamental material properties as well as dynamic effects of specimen-fixture interaction. Consequently, the impact strength measurement did not permit as detailed an interpretive analysis as might be desired, but it served as a very real measure of progress toward the goal of sufficient mechanical shock resistance for the turbine application. It is difficult to say precisely what value of impact strength is required for this application. A long range

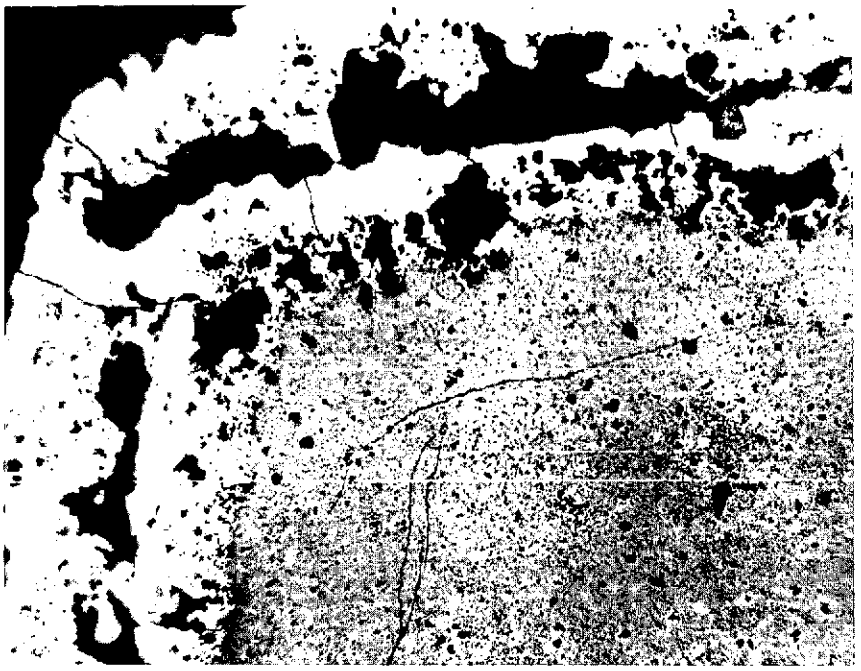

5782-1 100X

Figure 18. Sample R-3 Showing Reaction Sintered Si_3N_4 and Cap of Inconel 702 After Attempted Infiltration.

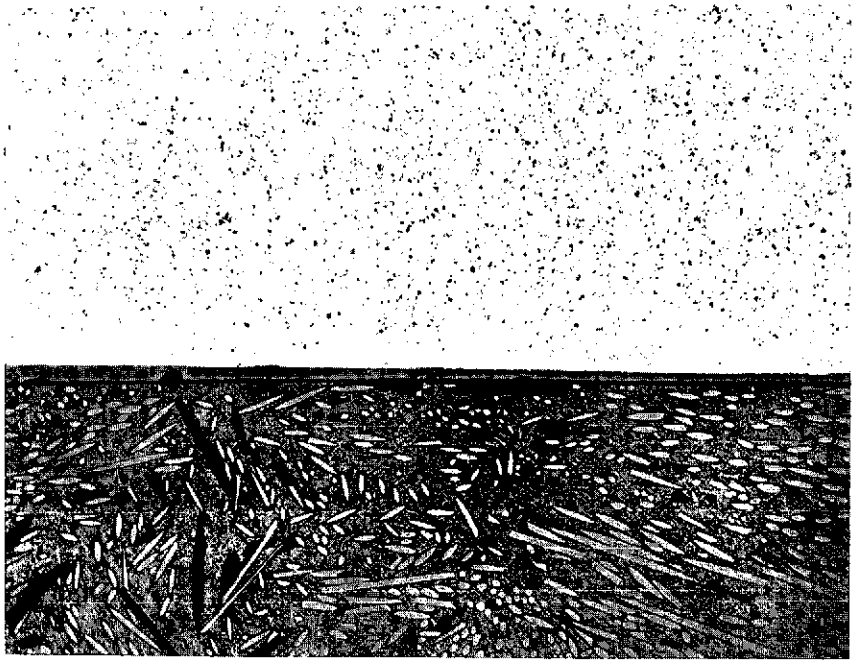

5792-1 100X

Figure 19. $LiAlSi_4O_{10}$ Glaze Coating on Hot Pressed Si_3N_4.

goal of 2-5 ft. lbs. and a short range goal of 6 ins. lbs. was established for this program.

After sufficient impact testing was accomplished to establish a promising material system, stress rupture testing was begun to determine if the material system had sufficient long term strength behavior to be of interest and learn if there was a correlation between this behavior, impact strength, and microstructure.

B. Mechanical Shock Resistance

A Bell Telephone Laboratories type impact tester was modified to provide impact strength data at temperatures from room to 2400°F (1589°K).(ref. 1) There is no standard test described for ceramic materials at elevated temperatures by the ASTM. However, the modified instrument does conform to the requirements of specification D256 - standard method of test for impact resistance of plastics and electrical insulating materials. The previous effort(ref. 1) provided comparison data of two superalloys; a nickel-base material - B1900, and a cobalt-base material - X40. The impact tester was modified to include some of the requirements of ASTM E23-66-Standard methods for notched bar impact testing of metallic materials. Specimens 0.250 inch (6.35×10^{-1} m) x 0.250 inch (6.35×10^{-1} m) in cross section, 2.165 inches (5.51×10^{-2} m) long with a 1.574 inch (4.00×10^{-2} m) gage length in a Charpy test mode were used. All the ceramic composite materials were unnotched and tested using a 2-foot pound (2.71J) hammer while a 16-foot pound (21.7J) hammer was used for the superalloys. Specimens were inserted into the hot furnace and soaked for 15 minutes prior to testing.

1. Monolithic Silicon Nitride, Silicon Oxynitride, and Silicon Carbide

Impact strength measurements for these materials are reported in Table VII. The Si_3N_4 data is graphically compared in Figure 20. All of the impact strength values exceed the 1969-70 results where β Si_3N_4 powder was employed. This is attributed to the use of α Si_3N_4 powder which results in higher strength material. The improved impact strengths over the 1971-72 results are attributed to improved powder processing; namely, the wet milling in t-butanol. Varying MgO concentration down to 1/8 wt. % MgO does not effect impact strength by a simple relation. However, it may be noteworthy that the highest elevated temperature impact strengths are for the lower MgO concentrations. Possible explanations for this behavior will be offered in subsequent sections.

The impact strength of Si_2N_2O, while not outstanding, was quite respectable considering the multiphase nature of the microstructure. This probably results from a fracture surface energy more related to Si_3N_4 than SiO_2.

SiC impact strengths are compared in Figure 21. Billet R2020 was extremely encouraging as the measured impact strengths were up to a factor of 6 higher than previous results(ref. 5) on SiC. The high density and fine grain size, features normally associated with high strength, were undoubtedly responsible for these results. In general, large grain size is detrimental. Billet R2019 had a duplex structure with numerous elongated grains up to 60 μm long. The impact strength of this billet fell off quite markedly at high temperature. It was surprising that the impact strength

TABLE VII

Impact Strength Results for Monolithic Materials

Billet	Material	Impact Strength, in-lb (Joules) Room Temperature	2000°F (1366°K)	2400°F (1589°K)
D1909	Si_3N_4 + 1/8 % MgO	3.16 (0.367)	2.36 (0.267)	3.03 (0.343)
D1870	Si_3N_4 + $\frac{1}{4}$% MgO	5.11 (0.580)	2.25 (0.255)	4.72 (0.534)
D1810	Si_3N_4 + $\frac{1}{2}$% MgO	2.24 (0.254)	4.50 (0.510)	3.14 (0.356)
D1872	Si_3N_4 + $\frac{1}{2}$% MgO	3.07 (0.347)	4.14 (0.468)	4.96 (0.561)
D1851	Si_3N_4 + 1% MgO	3.95 (0.448)	2.63 (0.298)	3.50 (0.397)
D1873	Si_2N_2O	1.76 (0.199)	2.97 (0.336)	3.35 (0.379)
D1837	SiC - Carbo + $1\frac{1}{2}$ w/o Al_2O_3 + $1\frac{1}{2}$ w/o C	2.87 (0.325)	1.30 (0.147)	1.59 (0.180)
D1860	SiC - Carbo + $1\frac{1}{2}$ w/o Al_2O_3 + $1\frac{1}{2}$ w/o C	2.52 (0.285)	2.36 (0.267)	1.23 (0.139)
R2020	SiC - Carbo + $1\frac{1}{2}$ w/o Al_2O_3 + $1\frac{1}{2}$ w/o C	4.66 (0.528)	5.29 (0.598)	2.36 (0.267)
D1823	SiC - PPG + $1\frac{1}{2}$ w/o Al_2O_3 + $1\frac{1}{2}$ w/o C	1.68 (0.190)	1.96 (0.222)	1.92 (0.218)
R2019	SiC - PPG + 1 w/o B + 1 w/o C	2.32 (0.262)	1.76 (0.199)	0.86 (0.097)

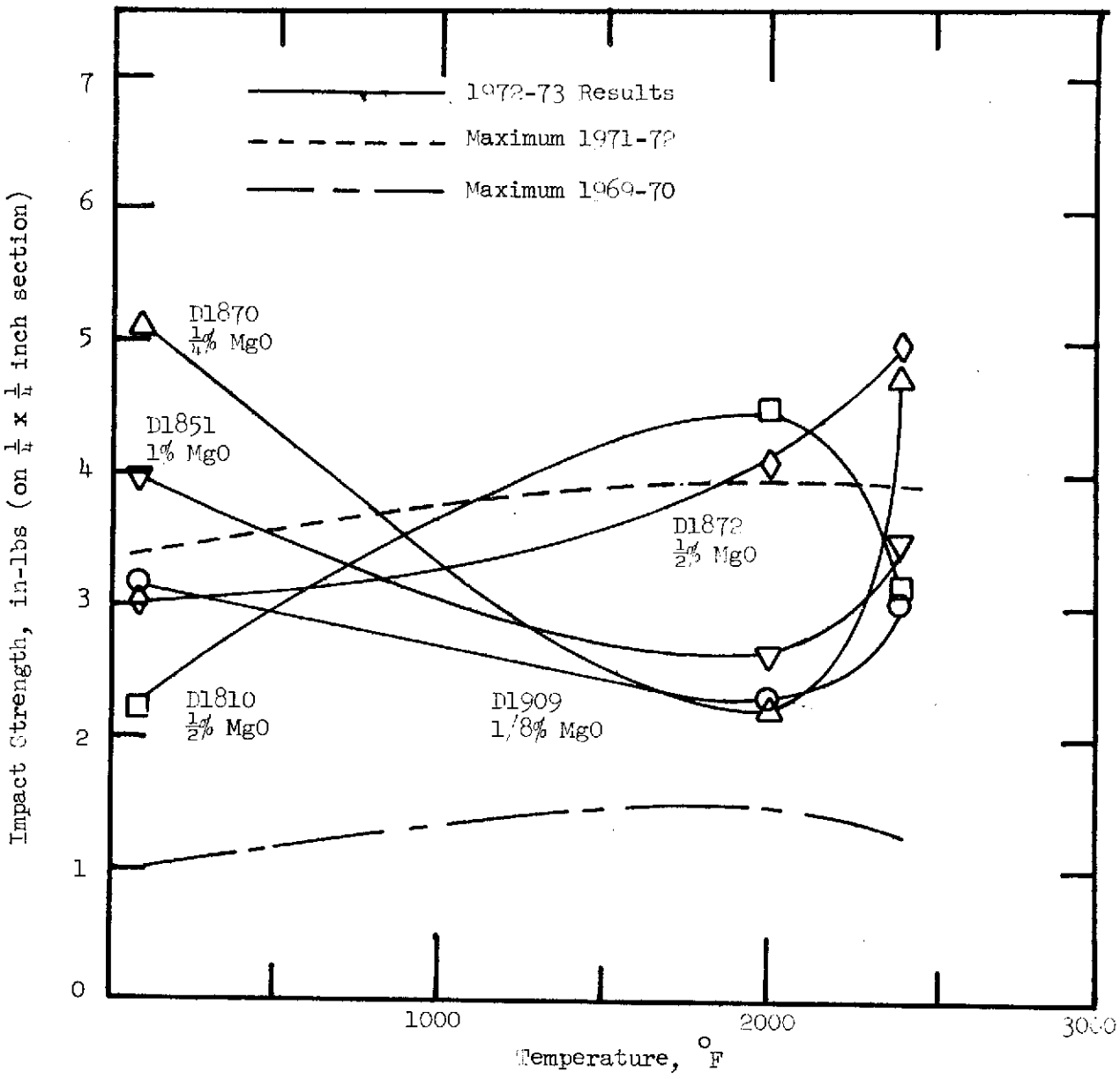

Figure 20. Charpy Impact Strength for Si_3N_4 as a Function of Temperature.

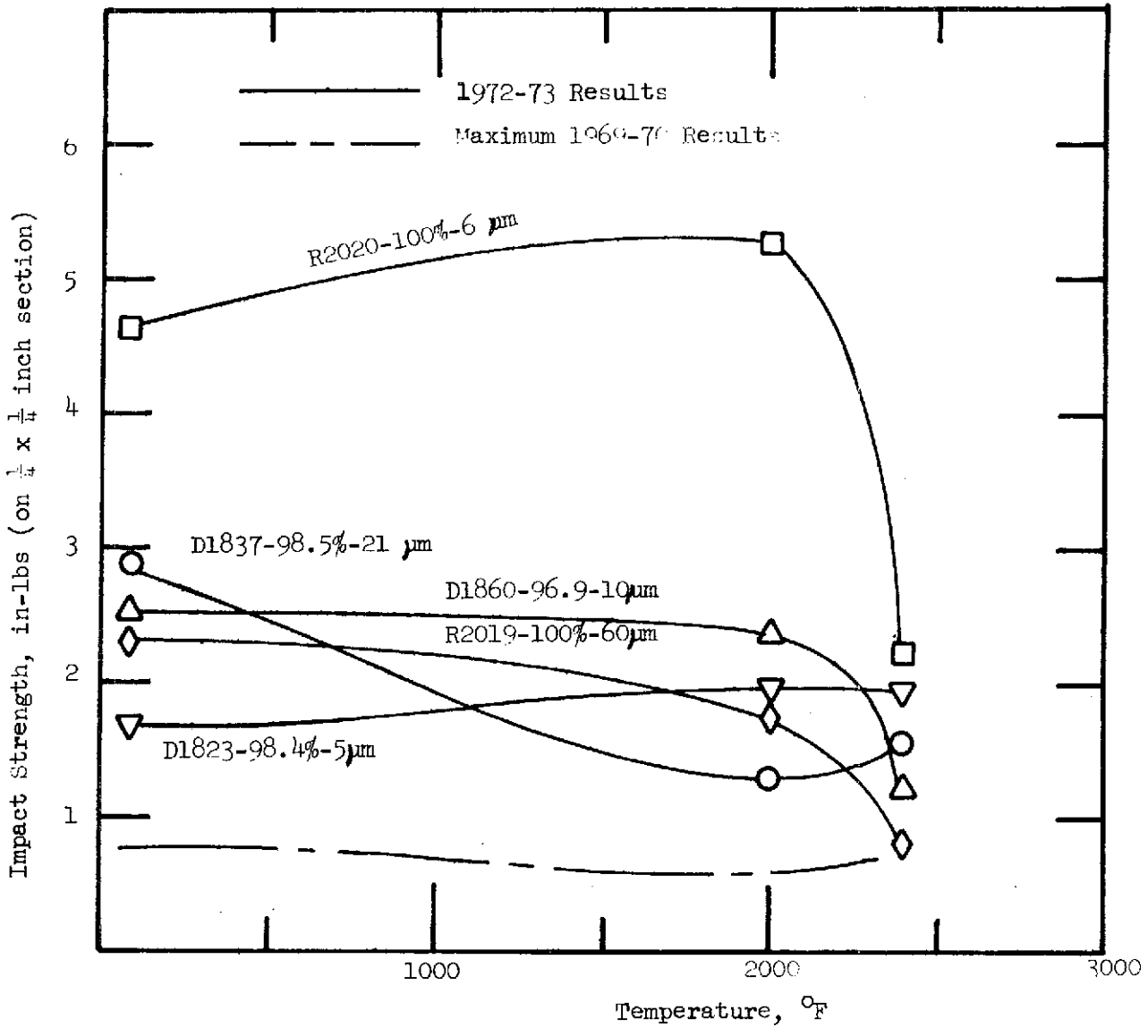

Figure 21. Charpy Impact Strength of SiC as a Function of Temperature.

was as high as it was at room temperature. Billet D1837, also with a large grain size, had a surprisingly high room temperature impact strength followed by a 50% reduction at elevated temperature. Billet D1823, which was 98.4% dense and fine grained, held a relatively constant impact strength with increasing temperature. This impact strength behavior is analogous with the normal SiC bend strength-temperature curve. It is expected that most of the impact strength-temperature curves would level out with improved testing statistics.

2. Composites

Impact strength measurements for the Si_3N_4/SiC particulate composite, D1814, and the Si_3N_4/wire composites are reported in Table VIII. The Si_3N_4/SiC composite had impact strengths well within the range of monolithic Si_3N_4 reported in Section IV.B.1. Apparently, the additional fracture surface energy associated with moving the crack front around the SiC particles was small compared with the energy consumed in the test, thus large improvements in impact strength were not realized.

The two Si_3N_4/superalloy wire composites had quite poor impact strengths. This result is not surprising based on the microstructural evaluation reported in Section III.C.1. Melting and silicide reactions were responsible for marked degradation of the Si_3N_4 matrix.

The Si_3N_4/Mo wire composites, Billet R2011, gave the highest impact strength measured in the current program. At room temperature the impact strength was on the low side for Si_3N_4 itself, and examination of the fracture surface showed no wire pull-out or evidence for plastic flow in the wires. This suggests that the wires were embrittled during fabrication or that a crack initiated in the sheath of Mo_5Si_3 had gained sufficient energy by the time it propagated into the Mo phase that plastic processes were inhibited. The fracture surface of the 8.33 in-lb 2000°F specimen is illustrated in Figure 22. It is apparent that both wire pull-out and wire deformation have contributed to the energy absorption. Fiber pull-out is a result of low interfacial shear strength between Si_3N_4 and Mo_5Si_3, resulting in part from the differential thermal contraction. The metallographic study demonstrated that the Mo_5Si_3 bonded to the Mo (Figure 15). Although the impact strength was not as high at 2400°F, the fracture surface demonstrated wire pull-out and plastic deformation. Billet R2010 containing 10 v/o of chopped random 0.005 inch dia. Mo had low impact strengths for three possible reasons; (1) the smaller wire diameter resulted in a larger volume of Mo_5Si_3, (2) the randomness and finite length (compared to the specimen dimensions) resulted in nonuniform residual stresses which probably gave undesirable tensile components on the surface placed in tension during the Charpy test, and (3) the nonuniform packing allows easy crack propagation paths.

The Si_3N_4/Ta composites did not exhibit the high impact strengths measured by Brennan and DeCrescente(ref. 6) for Si_3N_4/Ta composites fabricated at 1948°K. The microstructures of billets fabricated in this program (Figure 16) did show wire deformation as a result of fabricating at 10,000 psi and 1773°K. The reaction zone appeared less than or equal to the earlier work. However, the high Knoop hardness as reported in Section III.C suggested internal embrittlement which is probably responsible for

TABLE VIII

Impact Strength Results

Billet	Material	Impact Strength, in-lb (Joules)		
		Room Temperature	2000°F (1366°K)	2400°F (1589°K)
D1814	Si_3N_4 + SiC	2.29 (0.259)	3.94 (0.446)	3.22 (0.364)
D1894	Si_3N_4 + 13.4 v/o Ni20Cr	0.83 (0.094)	1.46 (0.165)	0.96 (0.011)
D1922	Si_3N_4 + 14.7 v/o Kanthol	0.64 (0.072)	0.91 (0.010)	0.55 (0.062)
R2010	Si_3N_4 + 10 v/o Mo	0.69 (0.078)	0.80 (0.090)	
R2011	Si_3N_4 + 13.7 v/o Mo	1.83 (0.207)	8.33 (0.943)	4.10 (0.464) 5.17 (0.585)
R2012	Si_3N_4 + 13.6 v/o Ta	1.23 (0.139)	1.89 (0.214)	2.03 (0.230)
R2021	Si_3N_4 + 15.9 v/o Ta	0.92 (0.10)	1.51 (0.171	2.43 (0.275)
D1933	Si_3N_4 + 6.3 v/o Re	0.77 (0.087)		
D1942	Si_3N_4 + 19 v/o Re		1.89 (0.214)	4.37 (0.495) 6.01 (0.680)

5839-4 10X

Figure 22. Fracture Surface of 8.33 in-lb Si_3N_4/Mo Composite Specimen Tested at 2000°F.

This page is reproduced at the back of the report by a different reproduction method to provide better detail.

not being able to confirm the potential for high impact strength in the Si_3N_4/Ta system.

The initial Si_3N_4/Re billet gave low impact strengths because of the delamination between layers as a result of a processing error. Billet D1942, however, resulted in the second highest impact strength measured on the program. The fracture surface (Figure 23) shows interfacial splitting and crack branching which undoubtedly accounts for the high impact strength. This composite was fabricated to serve as a model system for Si_3N_4/wire composites because of the low Re-Si_3N_4 reactivity. It was recognized that the high cost of Re would negate commercial exploitation of the system. The results demonstrate that wire composites can have high impact strengths. It is also clear that future work should concentrate on Si_3N_4/Mo, Si_3N_4/W(ref. 6), or Si_3N_4/Ta(ref. 6) for cost and performance considerations. The possible limitations on such systems by preferential oxidation of the metal can be circumvented through a design and fabrication route that eliminates exposed wires. Also, there is evidence(ref. 6) that the SiO_2 oxidation product of Si_3N_4 will form a protective coating over exposed wires.

3. Coated Si_3N_4

The impact strength for Si_3N_4 specimens coated with $LiAlSi_4O_{10}$ are compared with control specimens from the same Si_3N_4 billet in Table IX. In contrast to the earlier work on $LiAlSi_2O_6$ coating, no impact strength improvement was observed. This was surprising because the coating was visually of a much superior quality to the earlier glaze. The higher SiO_2 content of this glaze would result in a higher viscosity at a given temperature. If the contribution to impact strength was through shear in the coating upon impact, this could account for results noted. To carry this line of reasoning further, a low viscosity glaze would have little utility since it would not withstand the turbine environment.

4. Impact Failure Mode

Consideration of the failure mode for the impact test currently used gives an indication of the physical properties which effect the impact resistance. For ductile materials, impact strengths are commonly supposed to provide an indication of the work of fracture which is predominantly a result of plastic deformation. For the monolithic ceramics measured over the last three years,(ref. 1,5) normalizing the measured impact energies over the nominal fracture surface area gives values ranging from about 560 to 9,100 J/m^2 (0.40 to 6.8 in-lb). These values are from 10 to 200 times higher than any reasonable values of fracture surface energy, γ, measured for Si_3N_4 or SiC, demonstrating that these impact tests do not give a direct measure of γ for crack propagation.

The impact of brittle materials is more properly considered in terms of achieving a critical stress necessary to initiate motion of pre-existant flaws. Two distinct failure modes are generally possible for the levels of impact energy generally observed here.(ref. 11,12) One is initiation of cracks near the point of impact from local contact or Hertzian stresses.(ref. 13) The second is from longer range stresses resulting from elastic deflection of the body from the impact. These stresses are frequently flexural and often are substantially the same as would result from static loading to a similar load. For sufficiently flexible geometries, higher

5839-1 10X

Figure 23. Fracture Surface of 6.01 in-lb Si_3N_4/Re Composite Specimen Tested at 2400°F.

This page is reproduced at the back of the report by a different reproduction method to provide better detail.

Table IX

Impact Strength Results

Billet	Material	Impact Strength, in-lb (Joules) Room Temperature	2000°F (1366°K)	2400°F (1589°K)
1872	Si_3N_4 + 1/2% MgO	3.07 (0.347)	4.14 (0.468)	4.96 (0.561)
1872	As above W/LiAl Si_4O_{10}		3.97 (0.450)	4.90 (0.554) 3.75 (0.424)

vibrational stresses may result causing failure at lower impact energies than indicated for static loading.(ref. 14) The contact stresses generally do not affect the flexural stresses, although damage on the tensile surface from Hertzian cone cracks from previous impacts could lower the effective strengths.(ref. 15) Assuming rigid supports and neglecting loss energy imparted to the pieces, the impact energy is simply the elastic energy stored in the body at the instant fracture initiates. For the 3 point beam loading used in the Charpy test, this energy, U_e, is easily calculated to be:

$$U_e = \frac{2bha}{18} \quad \frac{\sigma^2}{E} = \frac{V\sigma^2}{18E} \tag{1}$$

where σ is the maximum tensile stress or fracture stress; E, the elastic modulus; h, the beam depth; b, the width; 2a, the length between supports; and V, the specimen volume under load.

Examination of the fracture surfaces of the impact bars indicated fracture initiated at the tensile surface and propagated back toward the impact surface as is to be expected for a flexural failure without vibrational problems. Further, for the higher impact strength bars, significant crack branching leading to multiple fractures frequently occurred indicating the stored elastic energy at initiation to be in excess of that needed to continue propagation.

For the standard Charpy test in which the hammer is dropped from a fixed height, excess energy is consumed as kinetic energy of the fractured pieces or toss energy. An upper limit to this energy can be calculated from the kinetic energy which would be transferred to the bar if it were free standing. For a massive hammer the limiting velocity of the piece would be

$$v = 2\, v_o \tag{2}$$

giving

$$U_T = \tfrac{1}{2}\, mv^2 = 2mv_o^2 \tag{3}$$

where m is the specimen mass, v_o the incident hammer velocity, and U_T the toss energy. For the specimens currently used and v_o = 11 ft/sec for the Charpy hammer, this maximum toss energy would be 1.4 in-lb; the toss energy may be less than this since the interference of the supports may lower it. In practice, the supports may not be rigid and additional energy may be transferred to them.

For all of the Si_3N_4 and SiC specimens from the past three years for which fracture strength and impact strength, I, measurements were available, the elastic strain energy, U_e, was calculated from equation (1) using the static fracture strength and compared to I in Figures 24 and 25. The strengths used were all taken from 4 point bend tests on 0.050 x 0.100 inch specimens tested on an 0.750 inch span with quarter point loading at a strain rate of 10^{-4} sec^{-1}. Sonic values of E from the literature(ref. 16) were used and taken as 45.5 x 10^6, 42.1 x 10^6, and 39.3 x 10^6 psi for Si_3N_4 at 72 °F, 2000°F, and 2400°F and for SiC 67 x 10^6, 63.8 x 10^6, and 62.8 x 10^6 psi for the same

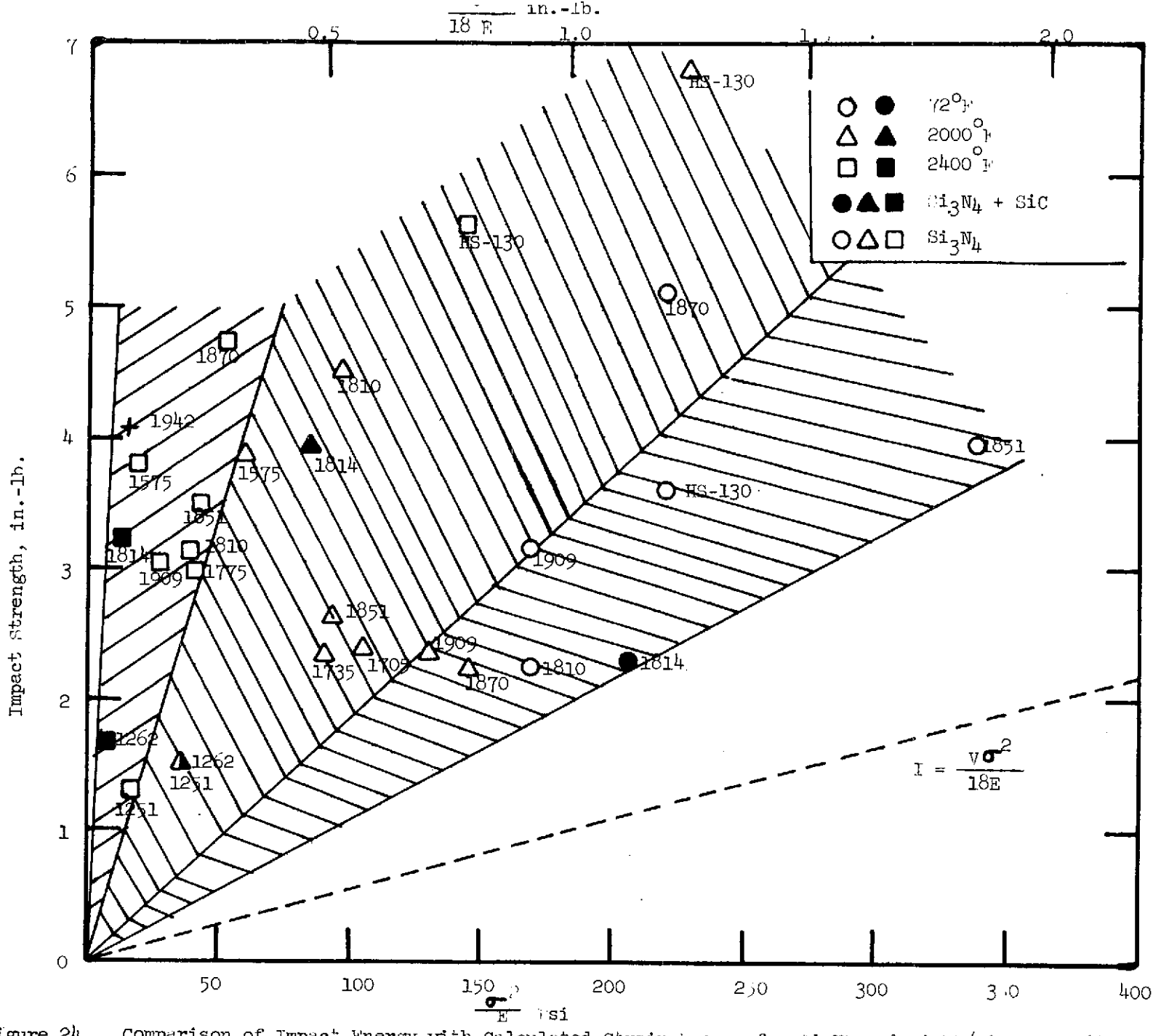

Figure 24. Comparison of Impact Energy with Calculated Strain Energy for Si_3N_4 and Si_3N_4/SiC Composite Specimens.

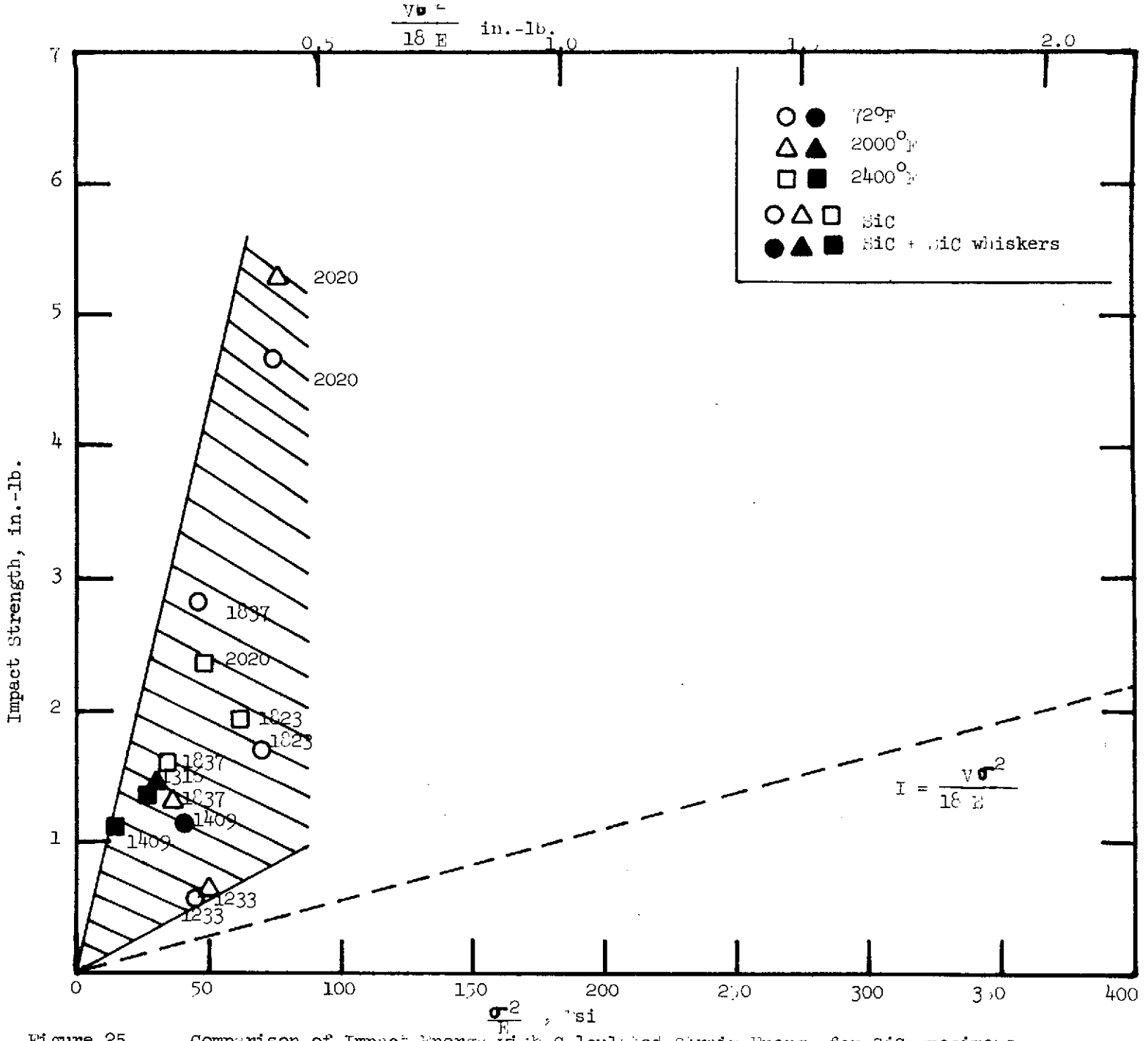

Figure 25. Comparison of Impact Energy with Calculated Strain Energy for SiC Specimens

temperatures.

Since the Charpy bars are larger, but are tested in 3 point flexure, the strength difference from size effects should be considered. The best fit to Weibull statistics for Si_3N_4 at low temperature reported by McLean, et al(ref. 16) gave a Weibull modulus of about 7 based on a surface area rather than a volume basis. Using this, the average strength for the two test modes should be nearly identical.

It can be seen that for Si_3N_4 the measured values of I at room temperature are 2-3 times the calculated values. Some of the discrepancy must certainly be toss energy as should be expected since the calculated maximum toss energy is an appreciable fraction of the measured values. However, the agreement with the calculated values is no better for the stronger specimens, where toss energy should be relatively less important; this indicates appreciable energy transfer to the supports must still be important. The general trend of results does, however, indicate a reasonable correlation between fracture strength and impact resistance. These results suggest better agreement between I and U_e would result from testing by incremental increases in hammer energy to avoid excess toss energies; such agreement has been reported for several other ceramics.(ref. 17)

At the higher temperatures the calculated values for Si_3N_4 are even lower, averaging about a factor of 6 too low at 2000°F and between 10 and 40 times too low at 2400°F. One possibility for this could be plastic deformation at high temperature since static and creep specimens exhibit appreciable deformation. However, it is more likely that at the strain rates involved in the impact tests there is little if any plastic deformation and that the static strengths used in the calculation are much too low. Support for this argument is found from the fracture surfaces which even at 2400°F are entirely brittle in appearance as shown in Figure 26. No evidence was seen in the impact fracture surfaces of the slow crack growth from grain boundary sliding seen previously(ref. 5) and by others(ref. 2) in lower strain rate tests on Si_3N_4. It is anticipated that at strain rates high enough to cause brittle fracture, the fracture strengths would be only slightly lower than the room temperature values; this would bring the agreement between I and U_e to within a factor of 2-3 and again provide a reasonable correlation between impact resistance and fracture strength. This view is also consistent with the lack of obvious dependence found between impact strength and temperature for the entire batch of Si_3N_4 materials. This correlation between strength and I indicates that surface treatments such as polishing or glazing will improve the impact resistance if the fracture strength is increased either by flaw removal or by compressive surface stresses.

For the SiC materials the agreement between the calculated and measured impact energy was less satisfactory. There was a positive increase in I with σ^2/E, but the impact energies were often as much as 10 times too high even at low temperature; further, there was much less difference between the high and low temperatures as anticipated since the high temperature strengths for SiC were generally similar to the room temperature values.

Some of the greatest discrepancies are found for the early composites where additions of SiC whiskers increased I and reduced σ compared to

This page is reproduced at the back of the report by a different reproduction method to provide better detail.

5839-5 10X

Figure 26. Fracture surface of 2400°F impact bar of Si_3N_4, 1909, indicating entirely brittle fracture with no slow crack growth or other evidence of plasticity. This brittle appearance was typical of all impact bars at 2000° and 2400°F.

comparable monolithic materials; this was initially suggested to result from microstructural interactions with the crack, but similar discrepancies with apparently monolithic SiC would seem to invalidate the argument. There is no obvious reason for this difference since strong strain rate effects on the fracture strength of SiC are not anticipated at low temperature. Better understanding of this problem would be useful to indicate further design considerations for this material under impact conditions or possible energy absorbing or fracture inhibiting factors not yet considered.

For the metal loaded composites the values of I were usually lower than for the better monolithic ceramics. This can be readily understood in terms of reduced strengths from defects due to reactions or porosity. Any increase in γ which may have resulted was insufficient to offset the effect of flaws on strength. For Mo and Re wire additions, some increases in impact strength were found. For these specimens the fracture surfaces indicated pull-out and deformation of the wires. This would contribute an appreciable amount to the work of fracture, i.e., γ to propagate a crack. For these materials a simple correlation between I and σ^2 is not expected. This is demonstrated for the Si_3N_4 + 19% Re, D1942, for which the room temperature strength was measured as 28 Kpsi. This value is plotted on Figure 24 using the average of the available impact tests which are at high temperature. It can be seen that the impact strength is much higher than would be expected based on σ^2/E even using the low temperature strength.

C. Transverse Bend Strength

Short time 4 point bend tests were performed in argon on specimens 0.875 x 0.050 x 0.100 inches with a 0.750 inch outer span and a 0.375 inch inner span. This provided a moment arm to half specimen height ratio of 7.5 which, although not the ideal value of 10, adequately imparts elastic bend conditions. The induction heated unit employed HfB_2 knife edge fixtures and a constant load rate which was set to provide a nominal strain rate of about 10^{-4} sec^{-1} assuming elastic behavior.

Tests were conducted on four Si_3N_4 billets fabricated with various concentrations between 1/8 - 1 wt. % of the MgO densification additive. Figure 27 shows, along with the strength versus composition curves at three temperatures, the relative density for each billet. The room temperature strength curve follows the density curve suggesting adherence to the Knudsen equation;

$$\sigma = \sigma_o \exp(-nP) \qquad (4)$$

where σ_o is the bend strength at zero porosity, P is the volume fraction porosity, and n is an empirical constant usually between 5-7. The 70°F data of Figure 27 best fit an n = 11 correction. This correction is higher than usually observed for oxides, but SiC and TaC have corrections in this range.(ref. 18) This implies that pores are severe stress concentrators. This is somewhat surprising since calculations based on fracture mechanics by Lange and Terwilliger(ref. 2) result in estimated flaw sizes of 80 - 180 μm. The observed pore size was 0.5 to 5 μm which leads to some uncertainty about the appropriate explanation for the 70°F strength dependency. The elevated temperature behavior exhibits a smaller strength dependence on concentration of MgO with 1/8 to 1/4 wt. % giving the best short

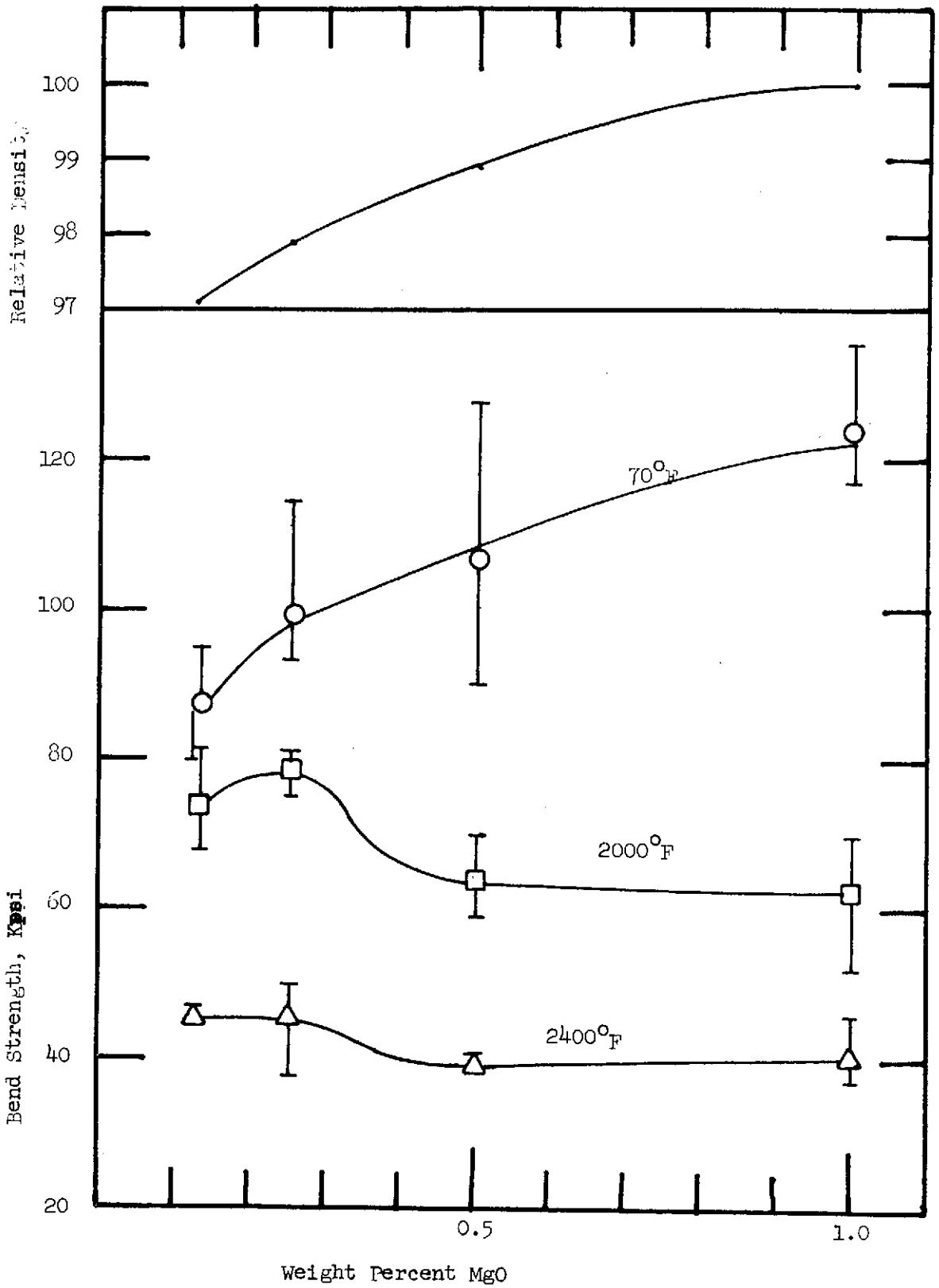

Figure 27. Strength at Three Bend Temperatures as a Function of MgO Addition.

time strength at 2000°F and 2400°F. It is thought that this may be a result of the MgO containing grain boundary phase being discontinuous in this concentration range. This structure would tend to inhibit grain boundary sliding and resultant cavitation. It is judged that the maximum in the strength-composition curve may shift for different levels of impurities in Si_3N_4 as some impurities, e.g., Ca, Na, and K, are thought to reside in the basically $MgSiO_3$ grain boundary phase.

Strength measurements on three SiC billets are illustrated in Figure 28. The two fine grained samples had about equal strengths, although there was more scatter in strength values for billet R2020. This scatter is attributed to the presence of isolated large grains in the microstructure. These grains probably have their origin in the powder, as noted in Section III.A.3. The high strength values at each temperature indicate considerable promise for SiC fabricated with PPG Industries' powder once powder uniformity and/or microstructure control is improved. The curve indicates a more severe fall off of strength with temperature for billet R2020 fabricated with Carborundum powder. It is uncertain whether or not this effect is real or due to the absence of tests in excess of 2400°F. The 19 μm grain size billet D1818 was about 25% weaker than the 5 and 6 μm material. This grain size (G) dependence is

$$\sigma \simeq K\, G^{-1/3} \qquad (5)$$

and is well within the range normally observed for ceramics. At high temperature the data for the two grain sizes appears to converge. This is further supported by previously unpublished data on a 18 μm, 99.1% dense SiC billet having an average bend strength of 48 Kpsi at 3272°F. Thus, at high temperatures, larger grain material may be beneficial due to increased resistance to creep and cavitation.

D. Stress Rupture

Testing was conducted in air under four-point bending mode using SiC for knife edge fixtures. The specimens were 1 - 3/4 x 0.100 x 0.200 inches with an outer span of 1.500 inches and an inner span of 0.500 inch. A predetermined load was applied smoothly in a few seconds with a cam accuator on the load bearing lever arm. Strain was not measured during testing, but was calculated based on final curvature on several specimens. A cut-off switch-clock circuit connected to the lever arm was utilized to detect and record failure. Short time tests were conducted to establish base line strength values. These tests were performed in argon on smaller specimens under conditions described earlier.

All of the results were analyzed using the elastic beam formula:

$$\sigma = \frac{3Pa}{bh^2} \qquad (6)$$

where: σ = transverse rupture strength in psi

P = load, in pounds required to fracture

b = specimen width in inches

h = specimen thickness in inches

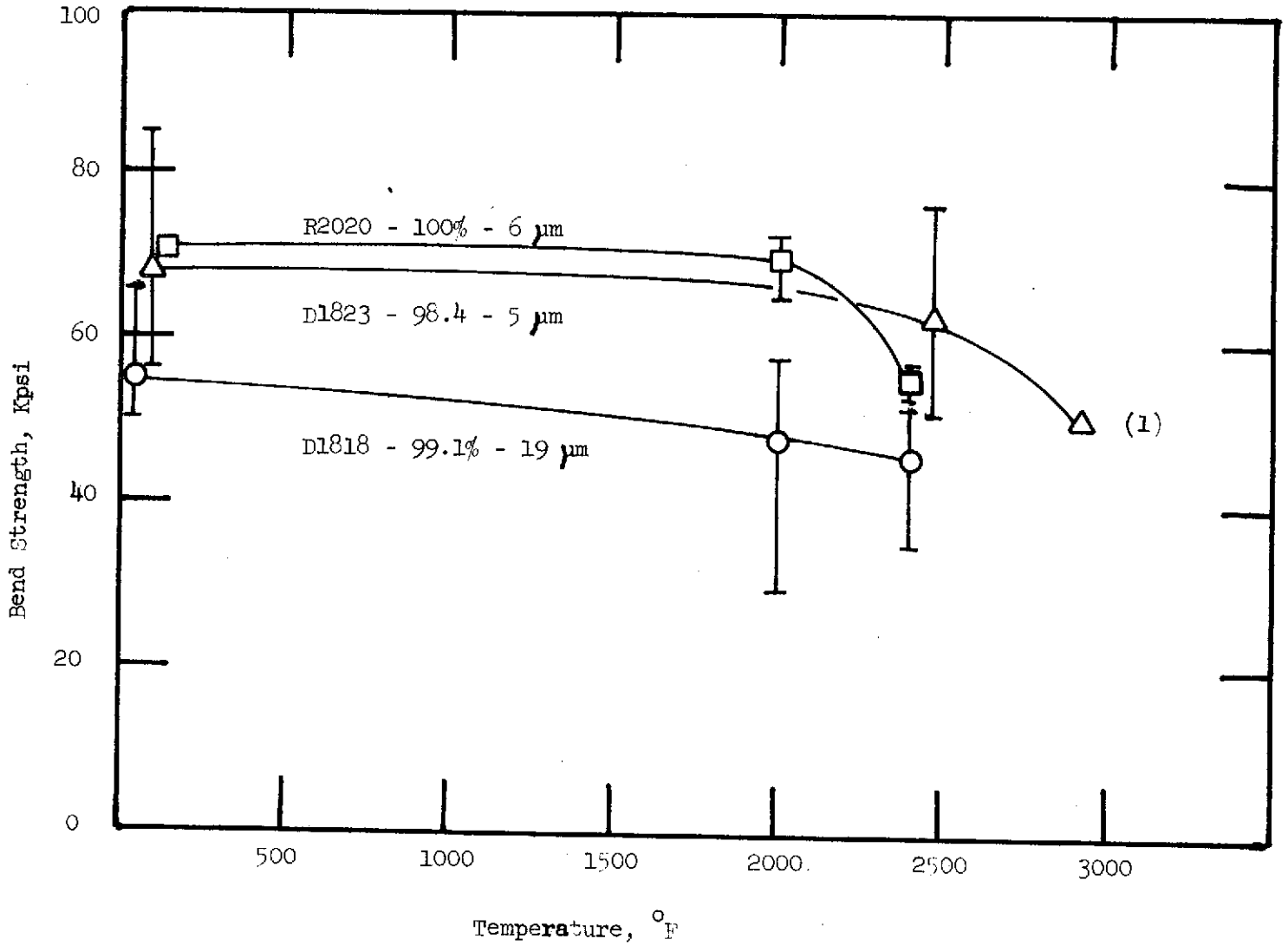

Figure 28. Bend Strength for Monolithic SiC as a Function of Temperature.

For a dead load test where plastic deformation occurs, an indication of the deviation from this formula can be obtained from the approximate equation for the steady-state stress:

$$\sigma = \frac{Pa}{bh^2} \quad (2 + m) \qquad (7)$$

where m is the strain rate sensitivity exponent. For metals, m is typically 0.2 to 0.3 so the stress will drop from its initial value to a value near that given by the above equation. For ceramics, m is typically between 0.5 and 1.0 so that there is often only a small difference between the actual steady-state stress and the calculated elastic stress.

Stress rupture tests were conducted on 100% dense Si_3N_4, billet D1851, fabricated with 1% MgO and 97.9% dense billet D1870 fabricated with $\frac{1}{4}$% MgO. The short time bend tests were discussed in Section IV.C. and it was noted that the lower MgO concentration resulted in higher average strengths at 2000°F and 2400°F. Stress rupture testing was conducted to see if this relation held. The data reported in Figure 29 includes the short time bend strengths which were measured in an argon atmosphere and on smaller test bars. The times plotted for the short time strength measurements are the time in which the specimen was within two standard deviations of the fracture stress. This was taken to approximate the period where cracks were subject to propagation. No corrections were made for variations in specimen size, although application of a Weibull volume correction indicates a 25% reduction of the short time strengths would be valid.

In contrast to the short time strength data, the 1% MgO billet had better stress rupture properties. The slopes for the two billets were more nearly equal at 2400°F, perhaps indicating a similar failure mechanism. However, the strain was markedly less for the 489 hr. 2400°F test on the $\frac{1}{4}$% MgO specimen compared with the 1% MgO specimen run at the same temperature and less than half the time (219.4 hrs.). This latter specimen was unbroken, but strained to the limit of the test fixture. The total strain of all of the specimens was compared semi-quantitatively, and this relation held; the lower MgO concentration inhibited deformation.

A microstructural examination (Figure 30) established that D1851 (1% MgO) and D1870 ($\frac{1}{4}$% MgO) had grain sizes of 0.78 μm and 0.95 μm, respectively. The grain morphology and texture appeared equivalent, and no conclusions could be made concerning the concentration or distribution of grain boundary phase. Both samples exhibited evidence for slow crack growth (SCG) and no marked differences in this behavior could be found. The grain size differences would predict increased creep rates for D1851, the 1% MgO sample, if the normal creep relations found in ceramics are followed. Increased creep rates were observed for this sample, but it is thought that the explanation encompasses composition as well as grain size.

Although there is no hard evidence to identify the operative creep mechanism, it is assumed that creep is controlled by grain boundary sliding and its accommodation which likely involves diffusion through the boundary phase. The stress rupture tests show that the 1% MgO samples had higher stress rupture strengths, higher creep rates, and lower short time bend strengths than the $\frac{1}{4}$% MgO samples. A major contributing cause of this behavior would appear to lie with improved accommodation with a commensurate

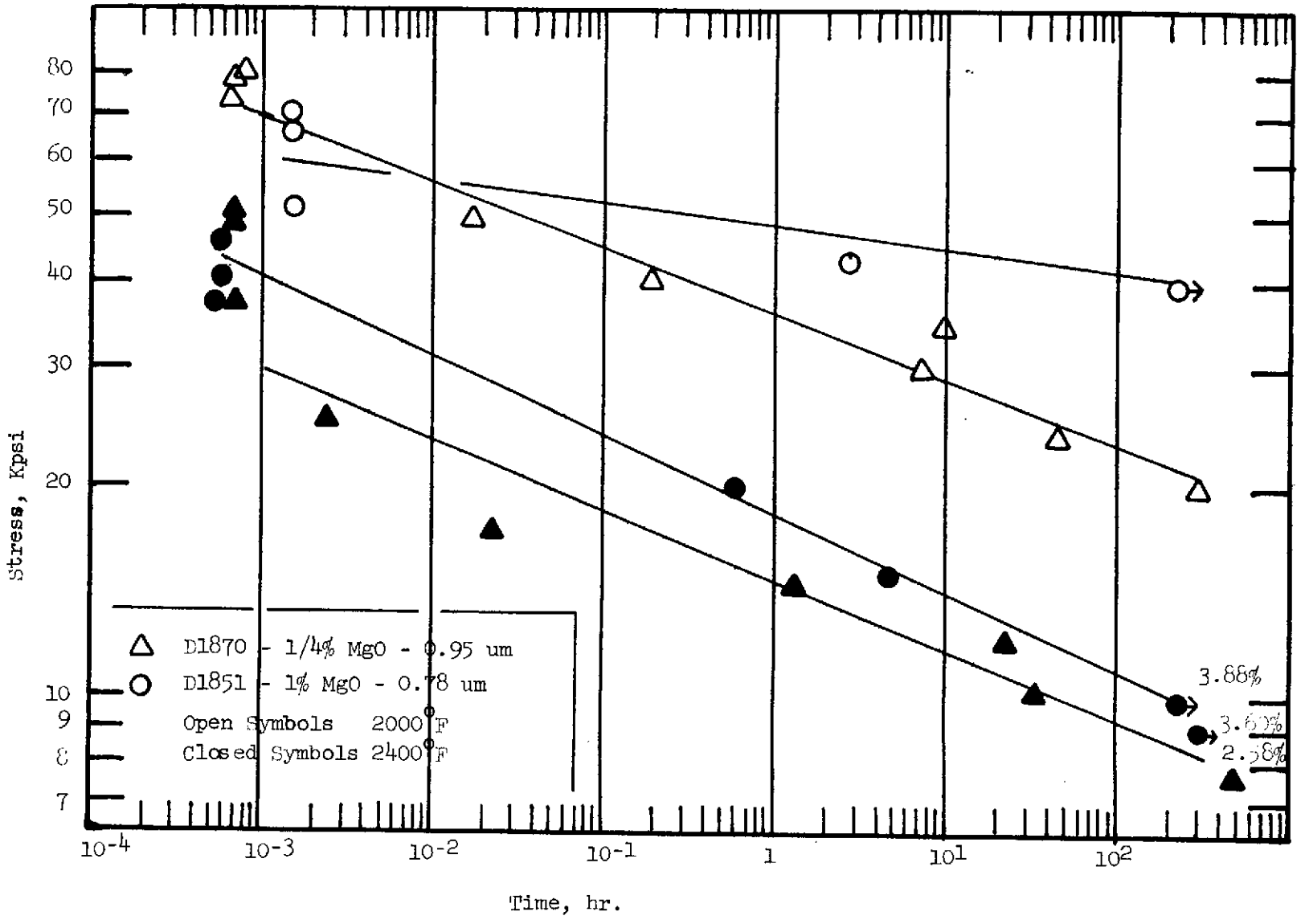

Figure 29. Bend Stress Rupture for Si_3N_4 with 1/4 w/o and 1 w/o MgO at 2000°F and 2400°F.

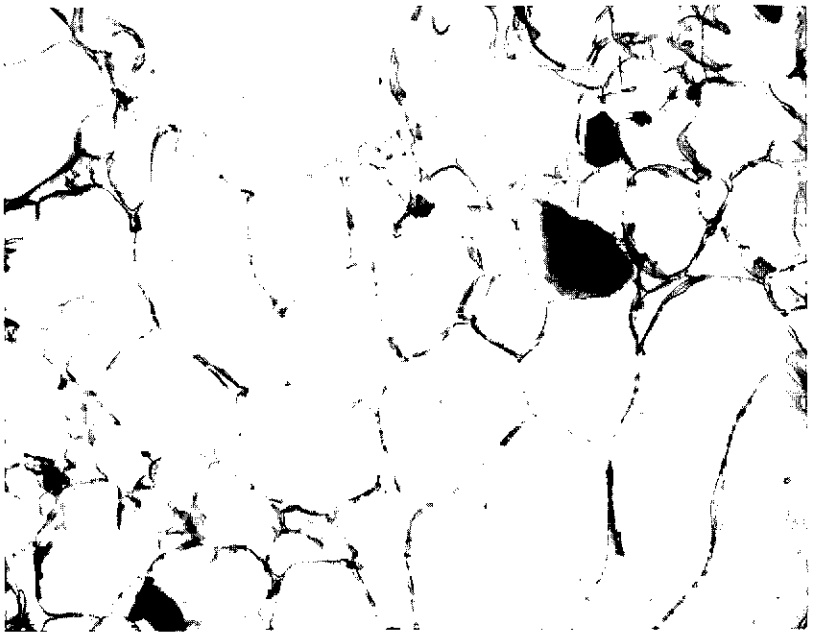

73084 (a) 15000X

73077 (b) 15000X

Figure 30 Grain Structure of (a) D1870 with $\frac{1}{4}$% MgO, and (b) D1851 with 1% MgO.

This page is reproduced at the back of the report by a different reproduction method to provide better detail.

reduction in cavitation for the 1% MgO composition. In other words, the 1% MgO material can achieve greater strains prior to the onset of and during slow crack growth. A possible explanation for this is that more of the boundaries contain $MgSiO_3$ resulting in an increased capacity for sliding and accommodation.

At low MgO content some of the boundaries have relatively less $MgSiO_3$ and are less able to accommodate the sliding due to the lower boundary diffusivity; such boundaries which are under tension are more likely to develop cracks. Further, the equilibrium dihedral angle for a pore which forms on a boundary with no $MgSiO_3$ may be lower especially if there is residual SiO_2 at the boundary or pore surface. Such a pore will have a lower curvature and so less resistance to further growth. The model based largely on composition is also consistent with the higher short time strengths for the $\frac{1}{4}$% MgO billet. The high strain rate allows the attainment of higher stresses prior to fracture for the $\frac{1}{4}$% MgO material because the importance of plasticity and accommodation is suppressed. This, in combination with the reduced creep rate for $\frac{1}{4}$% MgO material, causes the formation of the critical flaw to lag slightly over 1% MgO material resulting in higher measured short time strengths. Consequently, the compositional effects appear to be real and the desirability of a particular composition depends on the use and expected failure mode.

V. CONCLUSIONS

The major findings of this program are listed below:

1. Si_3N_4/Mo and Si_3N_4/Re wire composites had improved impact strengths over monolithic Si_3N_4. The improved properties were attributed to increased fracture surface energy due to plasticity and pull out of the wires. Although studies on Si_3N_4/Ta composites failed to substantiate the excellent results obtained by others, it is concluded that Si_3N_4/Mo, Si_3N_4/W and Si_3N_4/Ta composites warrant continued development. The high cost and modest results on Si_3N_4/Re account for the elimination of this system from the recommended list.

2. Alpha Si_3N_4 powder can be densified at as low as 1773°K providing 10 Kpsi hot pressing pressure is employed. Under more normal 2023°K - 4 Kpsi conditions, only 1/8 w/o MgO is required to attain 96.5% relative density and 1 w/o MgO is sufficient to give 100% relative density.

3. Si_3N_4 impact strengths were equal to, and in some cases, improved by 25% over previous results. The improvements were attributed to improved powder processing methods and possibly the use of low MgO additions. The 70°F impact strength was proportional to but higher by a factor of 2-3 than the elastic stored energy at the instant of fracture. At high temperature there was greater disagreement between the impact strength predicted by this model and the measured values, and this was attributed primarily to the effect of strain rate on strength.

4. The elevated temperature short time bend strength of Si_3N_4 is improved by employing 1/8 - 1/4 w/o MgO over additions up to 1 w/o probably because the $MgSiO_3$ grain boundary phase is incompletely

distributed which restricts grain boundary sliding. The bend stress rupture properties are better for the 1 w/o MgO material, however, and this is attributed to the increased accommodation and capacity for sliding prior to the onset of fracture which follows a period of slow crack growth. In contrast, the low temperature properties appeared to be more dependent on porosity than second phase with the less dense materials at low MgO content giving lower strengths.

5. 4 Kpsi SiC hot pressing conditions were identified which gave greater than 98% density for powders from three different vendors. The minimum grain size was 5 μm for one vendor's powder and the maximum grain size was 23 μm for a second powder. Increased densification kinetics were obtained at 10 Kpsi and a third vendor's powder which gave an intermediate grain size at 4 Kpsi was pressed to 100% density and 6 μm grain size under the higher pressure-lower temperature conditions.

6. SiC impact strengths were improved by up to a factor of 6 over previous results giving for the first time a SiC body equivalent to α derived Si_3N_4. There was little temperature dependence on impact strength which follows from a similar bend strength dependence. The disagreement with the predicted impact strength was about a factor of 10 in this case, and is not understood.

7. Short time bend strengths of up to 72 Kpsi were obtained for 6 μm grain size, high density SiC at 70°F and 2000°F. The fall-off in strength to 55 Kpsi at 2400°F suggested that larger grain size material (18 μm) with a nearly constant 50 Kpsi strength with temperature may prove desirable for stress rupture and creep considerations.

8. Although several superalloys wet SiC and Si_3N_4 the achievement of a good infiltrated structure does not appear feasible due to excessive reactions with the matrices.

9. A process was developed to achieve a $LiAlSi_4O_{10}$ glaze with an excellent visual appearance; however, impact strengths were not improved.

VI. REFERENCES

1. R.M. Cannon and R.J. Hill, "High Temperature Compounds for Turbine Vanes," NASA CR-72794.

2. F.F. Lange and G.R. Terwilliger, "Fabrication and Properties of Silicon Compounds," Final Report, Contract N00019-17-C-0107.

3. S. Wild, P. Grieveson, K.H. Jack and M.J. Latimer, Special Ceramics 5, The British Ceramic Research Association, Great Britain (1972), p. 377.

4. S. Prochazka, "Investigation of Ceramics for High Tempeature Turbine Vanes," Contract N00019-72-C-0129.

5. W.H. Rhodes and R.M. Cannon, Jr., "High Temperature Compounds for Turbine Vanes," NASA CR-120966.

6. J.J. Brennan and M.A. DeCrescente, "Fiber Reinforced Ceramic Matrix Composites," Contract N00019-72-C-0377.

7. B.W. Mott, "Micro-Indentation Hardness Testing," Butterworth Scientific Publication, London,(1956), p.249.

8. Thermophysical Properties of High Temperature Solid Materials, Vol. 1, Ed. Y.S. Toulokian, The MacMillan Co., New York (1967).

9. C.J. Smithells, Metals Reference Book, Vol. II, Butterworths, 1962, p. 893.

10. C. Goetzel, "Titanium Carbide-Metal Infiltrated Cermets in Cermets," edited by J.R. Tinklepaugh and W.B. Crandall, Reinhold Publishing Corp., New York (1960)., p. 130.

11. J.L. Glathart and F.W. Preston, "The Behavior of Glass Under Impact: Theoretical Considerations," Glass Tech., 9, 89 (1968).

12. J.P. Ashford and E.K. Priddle, "The Influence of Specimen Geometry and Structure on the Impact-Resistance of Silicon Carbides," Powder Met., 12, 169 (1969).

13. F.C. Frank and B.R. Lawn, "On The Theory of Hertzian Fracture," Proc. Roy. Soc., 299A, 291, (1967).

14. W. Goldsmith, Impact, Edward Arnold Ltd., London (1960).

15. A.G. Evans, "Strength Degradation by Projectile Impacts," J. Am. Ceram. Soc., 56, 405 (1973).

16. A.F. McLean, E.A. Fisher and R.J. Bratton, Brittle Materials Design, High Temperature Gas Turbine, AMMRC CTR-73-9.

VI. REFERENCES (Concl'd)

17. S.J. Acquaviva, "A Drop Weight Test for the Impact Strength of Ceramic Materials," Mat. Res. Stds., 11, 21 (1971).

18. R.W. Rice, Proceeding of the British Ceramic Society, 20, 205 (1972).

THE FOLLOWING PAGES ARE DUPLICATES OF ILLUSTRATIONS APPEARING ELSEWHERE IN THIS REPORT. THEY HAVE BEEN REPRODUCED HERE BY A DIFFERENT METHOD TO PROVIDE BETTER DETAIL